11-29-2005

Reactivity Study of Platinum Nanoparticles and Nanowires Inside the Channels of Mesoporous Silica

Marcus R. Smith

THE UNIVERSITY OF NEW MEXICO
ALBUQUERQUE, NEW MEXICO 87131

POLICY ON USE OF THESES AND DISSERTATIONS

Unpublished theses and dissertations accepted for master's and doctor's degrees and deposited in the University of New Mexico Library are open to the public for inspection and reference work. *They are to be used only with due regard to the rights of the authors.* The work of other authors should always be given full credit. Avoid quoting in amounts, over and beyond scholarly needs, such as might impair or destroy the property rights and financial benefits of another author.

To afford reasonable safeguards to authors, and consistent with the above principles, anyone quoting from theses and dissertations must observe the following conditions:

1. Direct quotations during the first two years after completion may be made only with the written permission of the author.

2. After a lapse of two years, theses and dissertations may be quoted without specific prior permission in works of original scholarship provided appropriate credit is given in the case of each quotation.

3. Quotations that are complete units in themselves (e.g., complete chapters or sections) in whatever form they may be reproduced and quotations of whatever length presented as primary material for their own sake (as in anthologies or books of reading) ALWAYS require consent of the authors.

4. The quoting author is responsible for determining "fair use" of material he uses.

This thesis/dissertation by Marcus R. Smith has been used by the following persons whose signatures attest their acceptance of the above conditions. (A library which borrows this thesis/dissertation for use by its patrons is expected to secure the signature of each user.)

NAME AND ADDRESS	DATE

Marcus R Smith
Candidate

Chemical and Nuclear Engineering
Department

This thesis is approved, and it is acceptable in quality and form for publication on microfilm:

Approved by the Thesis Committee:

Bruce Bates, Chairperson

Thomas B. Thoy

William J. Kroenke

Accepted: Amy B. Wohlert
Dean, Graduate School

NOVEMBER 29, 2005
Date

REACTIVITY STUDY OF PLATINUM NANOPARTICLES AND NANOWIRES EMBEDDED INSIDE THE CHANNELS OF MESOPOROUS SILICA

BY

MARCUS R. SMITH

B.S., CHEMISTRY, UNIVERSITY OF ARIZONA, 1998
B.S., MATERIALS SCIENCE AND ENGINEERING, UNIVERSITY OF ARIZONA, 2000
M.S., CHEMICAL ENGINEERING, UNIVERSITY OF NEW MEXICO, 2005

THESIS

Submitted in Partial Fulfillment of the
Requirements for the Degree of

Master of Science
Chemical Engineering

The University of New Mexico
Albuquerque, New Mexico

December, 2005

REACTIVITY STUDY OF PLATINUM NANOPARTICLES AND NANOWIRES EMBEDDED INSIDE THE CHANNELS OF MESOPOROUS SILICA

BY

MARCUS R SMITH

ABSTRACT OF THESIS

Submitted in Partial Fulfillment of the
Requirements for the Degree of

Master of Science
Chemical Engineering

The University of New Mexico
Albuquerque, New Mexico

December, 2005

REACTIVITY STUDY OF PLATINUM NANOPARTICLES AND NANOWIRES EMBEDDED INSIDE THE CHANNELS OF MESOPOROUS SILICA

by

Marcus R Smith

B.S., Chemistry, University of Arizona, 1998

B.S., Materials Science and Engineering, University of Arizona, 2000

M.S., Chemical Engineering, University of New Mexico, 2005

ABSTRACT

Pt metal nanowires and nanoparticles were prepared using mesoporous silica as the template. Mesoporous silica with straight 1-dimensional, tortuous 1-dimensional and 3-dimensional channels was used. The experimental techniques included CO oxidation, Chemisorption, XRD, and STEM. CO oxidation and chemisorption provided the data to calculate the intrinsic reactivity, known as turn over frequency (TOF). Powder XRD was used to measure line broadening. The FWHM of the XRD line broadening was used with the Scherrer formula to determine Pt metal crystallite size. STEM images permitted for the measurement of the particle diameters, and the determination of morphology.

Two commercially available reference samples were used to provide a benchmark for comparison, namely Pt on alumina and Pt on

silica. The resulting TOF of these reference catalysts were identical, confirming that the CO oxidation reaction is structure insensitive.

Pt metal loading was achieved by impregnation of the mesoporous silica with $PtCl_6^{2-}$ in an aqueous solution. After evaporating the solution, the remaining powder was reduced under flowing hydrogen at 200°C for 2 hours. This method resulted in predominantly Pt nanoparticles. During reduction, a second method of saturating with H_2 was used to achieve Pt metal nanowires embedded within the silica mesoporous framework. The second method involved bubbling the flowing hydrogen through water to saturate the reducing hydrogen gas. This method creates a volatile Pt complex that easily transports throughout the mesoporous framework. The methods used to develop predominately nanoparticles and nanowires through the reduction process, were shown successful yielding samples with very different morphologies. Pt metal nanowires and nanoparticles have similar CO oxidation, and chemisorption data. This indicates that both nanowires and nanoparticles were readily accessible to hydrogen uptake. The TOF data indicates that the samples tested had similar accessibility to hydrogen.

TABLE OF CONTENTS

LIST OF FIGURES

LIST OF TABLES

CHAPTER 1

Introduction

1.1 Goals and Objectives

Heterogeneous catalysts are used to catalyze gas phase reactions such as CO oxidation for pollution control, methanol synthesis to provide us with chemicals and Fischer-Tropsch synthesis to provide alternative energy sources. In these catalysts, the reactivity is confined to the surface of the solid phase. Catalysis is a surface phenomenon, which is dependent upon the availability of active surface sites. The greater the number of active surface sites, the higher the reactivity. To increase reactivity per gram of catalyst, and to achieve high Pt surface areas, catalysts are prepared with the smallest possible Pt crystallites. However, nanosized crystals have a tendency to grow in size through coalescence or ripening, leading to a loss of surface area. By stabilizing the nanoscale structures in the pores of silica, it may be possible to control the thermal sintering of these catalytic materials.

Engineered powders of silica, with controlled mesoporous channel diameters, provide a template to control the morphology of deposited Pt crystallites. Mesopores of diameters of 3 nm (MCM-41) and 7 nm (SBA-15) arranged in hexagonal arrays provide one class of 1-D hexagonal mesoporous silica (Beck, 1992; Zhao 1998). Another type of silica structure (SBA-11) is characterized by 3-D interconnected mesopores with many intertwined channels (Zhao, 1998). A third type of silica (aerosol derived silica) has channels spiraling continuously within spherical silica particles (Bore, 2004). Aerosol particles have no detectable pore surface openings.

Wet impregnation works equally well with each type of silica to achieve controlled Pt weight percent loading. Depending upon the mobility of the Pt ionic salts during reduction, the Pt will either form nanoparticles or can be made to form nanowires. Pt nanowires prepared in this manner have successfully been used to image pore structures in cubic and 3-d hexagonal mesoporous silica (Terasaki, 2002; Guo, 2005; Han, 2000; Fukuoka, 2001a; Fukuoka 2001b). Since the pores are completely filled by the Pt, the Pt takes the shape of the channel. The nanowires are especially interesting since they may provide greater thermal stability than the nanoparticles.

All of these nanostructures are located within silica pores and in some cases fill the pore completely. Hence a major question remains: will these nanowires be accessible to the gas phase and be catalytically active? The principal objective of the study was therefore to determine the reactivity of Pt nanowires confined within silica pores and to compare the intrinsic reaction rates with Pt nanoparticles in more conventionally prepared Pt catalysts. Two Important parameters of interest in catalytic studies are total reactivity per gram catalyst and the intrinsic reactivity, turn over frequency (TOF), which represents the molecules reacted per surface site (Boudart, 1995). If the Pt in mesoporous silica is found to have TOF comparable or better than the reference catalysts, it would be of great interest as a heterogeneous catalyst. Future work can be then be directed to investigating the thermal stability of these confined nanostructures.

1.2 Motivation for This Study

Nanoparticles can lose surface area due to coalescence or ripening. Mesoporous silica has the potential of playing an important role in preventing coalescence and ripening. The ability of crystallites to migrate is dependent on the wetting angle between

the metal particle and substrate (Dorling, 1971). Silica is a non wetting support and would tend to promote particle migration. But when the Pt crystallite is confined within a pore, its ability to migrate is limited, particularly when its diameter approaches the pore diameter (Chen, 1978). Hence, the porous silica may have the ability to restrict particle migration and coalescence.

The driving force for Ostwald ripening is surface free energy. Differences in the mean adatom concentrations in the vicinity of small and large particles leads to diffusion controlled growth (Boudart, 1971). According to the Gibbs-Thompson equation, nanometer sized particles are inherently unstable since the small radius of curvature leads to an enhancement in the chemical potential. For a nanowire, the radius of curvature in one direction is infinity, and this will tend to reduce the chemical potential of surface atoms compared to that of nanoparticles of equal size. Since the fugacity of the particle via the Gibbs-Thompson equation is related to an exponential of the inverse of radius of curvature, nanowires may be more stable than the nanoparticles.

The question remains as to whether the nanowires will be as reactive as the nanoparticles. Since the nanowires are confined within mesoporous channels, and in immediate proximity to the silica substrate, they might be expected to exhibit lower activity, particularly if the surface sites are blocked by the silica. In this case Pt nanoparticles confined deep within the channels would be inaccessible to reactive gases. On the other hand, Fukuoka, et. al. have suggested that nanowires are actually more reactive than nanoparticles for water gas shift and for butane hydrogenolysis (Fukuoka, 2001a; 2001b). The authors suggested the reason for higher reactivity was the electron deficiencies of the nanowires relative to the nanoparticles, as measured by XAFS and

XANES techniques. In this work, we have used the CO oxidation rate as a probe reaction, since this reaction is structure insensitive and would not be expected to be influenced by any metal-silica contact. Furthermore, previous work has not reported any direct comparisons of TOF between conventionally prepared catalysts. In this study, we used two reference catalysts to provide a benchmark for comparison of the reactivity of nanowires and nanoparticles.

CHAPTER 2

Review of Literature

2.1 Mesoporous Silica Synthesis

The synthesis of highly ordered, mesoporous silica is achieved from solutions of surfactants and silica soluble precursors. The morphology of the mesoporous materials is controlled during the self-assembly of the molecular organic and inorganic species. Triblock copolymers form hexagonal mesostructures, and nonionic oligomeric ethylene oxide surfactants form cubic phases. In acid media, hydronium ions associate with the alkylene oxygen atoms to facilitate long-range polymer order with coulombic interactions. The structure is defined by the organization of the surfactant molecules into micelles which serves as the templates for the mesoporous structures. Encapsulation occurs because anionic inorganic species and the cationic hydrophilic surfaces of the micelles form from the surfactant. The surfactant liquid crystal structures which form are sensitive to solution conditions such as: ionic strength, counterion polarizability, surfactant concentration, counterion charge, temperature, and the addition of co-surfactants or additives like alcohol or hydrocarbons (Beck, 1992).

In the case of SBA-15, poly(ethylene oxide)-poly(propylene oxide)-poly(ethylene oxide) (PEO-PPO-PEO) (Aldrich P123) copolymers are used as the surfactant. A dilute aqueous concentration of tetraethylortho silicate (TEOS) provides the silica phase. Under slightly acidic conditions at room temperature for 20 hours, silica dioxide powder precipitates with hexagonally arranged pores (Stucky, 1998).

In the case of cubic SBA-11, $C_{16}H_{33}(OCH_2CH_2)_{10}OH(C_{16}EO_{10})$ (Aldrich Brij 56) surfactant species were used. CTAB and sodium silicate furnished the silica.

Calcination provided the siloxane condensation, which improves the long range order of the mesophase (Stucky, 1998). The mesopores are arranged in 3-dimensional hexagonal structure.

Beck et. al developed a family of mesoporous molecular sieves they designated M41S (Beck, 1992). Of these, MCM-41 contains hexagonally arranged pores with long range order and controlled pore diameters. Through adjusting the concentrations of the precursor materials, the channel sizes were varied. The synthesis was a liquid crystal template mechanism using tetramethylammonium silicate and teteraethylortho silicate. Within the solvent, silica forms inorganic walls between surfactant liquid crystal structures from a quaternary ammonium surfactant compound, such as CTAB. As-synthesized MCM-41 materials contain surfactant molecules arranged in a micellular array. Powder X-ray diffraction data of the synthesized material was consistent hexagonal structure.

Aerosol hexagonal mesostructures were produced by the evaporation-induced self-assembly (EISA) aerosol technique (Bore, 2003). Round silica particles with worm-like mesostructures were synthesized using the EISA aerosol method and an acidic aqueous solution with the surfactant CTAB. Uniform channels were synthesized by varying the ratio of precursor materials, and pH. The aerosol droplets are evaporated in a tube furnace of 0.6 meters length at a temperature of 125°C with flowing N_2 at 3.6 slpm. The precursor solution was mixed with DI water and 1 N HCl before adding the TEOS. The resulting powders were collected on filter paper. Powders were calcined at 500 °C for 12 hrs. TEM images show the particles contain pores that do not appear to terminate

at the silica surface. The pores appear ordered with respect to each other as they are seen to swirl about immediately under the surface.

2.2 Synthesis of Nanowires

A number of studies have been conducted with the intention of TEM imaging mesoporous channels of SBA-15 and MCM-41 containing Pt nanowires. The TEM imaging of SBA-15 show the mesopores contain wires interconnected by microscopic bridges. This suggests that for SBA-15 there is microporosity between the mesoporous channels (Zou, 1998). The Pt nanowires have lengths on the order of several tens to several hundreds of microns (Ryoo, 2002). Nanowires have good crystallinity and smooth surfaces. The lattice fringes suggests that they consist of single crystals.

Pt nanowires in SBA-15 showed well ordered, hexagonal arranged 1-D pores of uniform size (Han, 2000). $Pt(NH_3)_4(NO_3)_2$ was incorporated into the silica by the incipient wetness technique. Solvent was evacuated under vacuum and CH_2Cl_2 was added to induce outer surface Pt to form within the pores. The impregnated powder was dried under room temperature and reduced under H_2 flow at 593 K. The Pt wires retain their structural integrity after treating the silica with HF.

Stucky et. al. also prepared Pt nanowires with SBA-15 to observe the mesoporous structure (Stucky,2000). Two-dimensional micrographs recorded at tilts of –60 and 60 degrees allowed the development of a 3D image (Han, 2000). The Pt conforms to the shape of the mesopores by forming nanowires approximately 0.5 μm long with diameters of 7 nm. Silica was dissolved, and the nanowires retained their shape based on TEM imaging.

In one technique for forming Pt nanowires inside MCM-41, the Pt source was $[Pt(NH_3)_4]NO_2$ to give the $Pt(NH_3)_4^{2+}$ incorporated into the mesopores by impregnation (Ryoo, 2000). After filtration and drying, the Pt was activated in a stream of O_2 at 320°C. This was followed by reduction in a stream of H_2 at 300°C. The reduced Pt formed the seeds for additional loading of Pt. The Pt loaded powder was mixed with an aqueous solution of $Pt(NH_3)_4NO_2$ to give additional loading to a total of 5 wt. % Pt. After filtration, the sample was again reduced in H_2 at 300°C for 2 hours with a ramp rate of 4 hours. Nearly all of the Pt metal was incorporated into the silica channels, with Pt particles also observed on the external surface (Ryoo, 2000). The values of the d spacing imaged with HREM, indicate that the nanowires show {111} and {200} planes of Pt. The face-centered cubic structure of Pt preferentially grows along the <110> axis. Guo et. al. synthesized Pt nanowires in channels of cubic mesoporous silica. In MCM-48 (Ia3d symmetry) with interconnected pores, TEM show pore diameters of 2.6 nm (Guo, 2004). A 5 wt. % loading was achieved by mixing a slurry of silica with H_2PtCl_6 at room temperature using the wet impregnation technique. The powder was reduced under flowing H_2 at 300°C to form localized regions of Pt rod structures inside the channels. Where channels interconnected, the Pt formed tripod like structures that conformed to the 3D structure of the mesopores. The accessibility to air of the nanomaterials was determined by XAFS. Pt nanowire formation was highly dependent upon atmosphere during reduction. Pt nanowires embedded in mesoporous MCM-48 cubic structure did not oxidize in ambient air (Han, 2000).

Photo reduction was later used to form Pt nanowires within the framework of mesoporous silica by Fukuoka et. al. Fukuoka characterized the synthesis of Pt

nanowires in inorganic silica mesoporous FSM-16. Pt nanowires were produced inside the pores by salt impregnation, followed by reduction under photo- and gamma-ray irradiation. Solutions of FSM-16 were impregnated with H_2PtCl_6 to a loading of 5-10 wt.%. Water and methanol vapors, added to the Pt impregnated sample of 5 wt. % Pt caused the Pt ions to migrate through the channels of the mesopores. The Pt ions were catalytically reduced to form wires. Fuokouka postulates that $PtCl_6^{2-}$ ions migrate to the vicinity of the nanoparticles where they are reduced on the surface of these structures and elongate along the channels of the pores (Sasaki, 2001). In water-gas shift reactions, nanowires are found to be more reactive than nanoparticles. The conclusion is that the morphology of nanowires influences the electronic state of surface atoms.

In the case of wires, the lattice fringes from HRTEM and electron diffraction of the Pt nanowires indicated that the wires are single crystals. The Pt wires formed along the 1-D channels conformed to the pore size of the substrate. XAFS and XPS showed that the Pt wires were slightly electron deficient compared to the Pt particles. The formation mechanism proposed suggests that small nanoparticles initially form and $PtCl_6^{2-}$ ions successively reduced on the particles to grow to wires under UV-Irradiation.

Bore incorporated Pt nanowires into aerosol silica using $H_2PtCl_6*6H_2O$. The method involved forming a slurry of silica suspended in a solution of DI water. $H_2PtCl_6*6H_2O$ was added, to give a weight loading of 5 wt. %. Under vacuum, the solution was dried to a fine yellow powder consisting of the anionic salt of Pt embedded into the silica. The anion was reduced under a H_2 flow at 200°C for 2 hours, with a ramp time from room temperature of 4 hours. When the flowing hydrogen was saturated with DI water, wires formed. The Pt agglomerates into localized regions to form the

nanowires under wet reduction. When particles formed, they were evenly distributed throughout the sample. This suggests that the Pt precursor had higher volatility under wet reduction, and was more easily transported through the tortuous paths of the mesopores to elongate into nanowires.

2.3 Reactivity of Pt Nanowires

Catalytic performance of Pt nanowires and Pt nanoparticles in mesoporous silica channels using the water-gas-shift reaction were compared (Fukuoka, 2001b). The formation of CO_2 at 373 K was measured. Pt wires showed higher reaction rates, in spite of containing fewer surface atoms than the catalysts containing Pt nanoparticles. TOF was evaluated based on the surface Pt atoms using a 2:1 hydrogen to Pt stoichometery. The hydrogen uptake was determined by chemisorption. The TOF was 1.01 hr^{-1} for wires and 0.126 hr^{-1} for particles at 73 K. This is explained by the nucleophilic attack of H_2O on CO adsorbed on Pt for wires, owing to the electron deficiency to the surface of the pt wires, as observed by XAFS.

Fukuoka compared the hydrogenolysis of butane over Pt nanowires and Pt nanoparticles. The TOF for the wires was substantially higher than that of the particles, in spite of a smaller surface area. The reason for the higher activity was attributed to the higher electron deficiency of the wires (Fukouka, 2001a)

Nanowires formed within the channels of mesoporous silica have been shown to be electron deficient relative to bulk Pt and to Pt nanoparticles (Fukouka, 2001a). This characteristic has been used to explain the improved turn over frequency (TOF) reported in Pt catalysis for hydrogenolysis of butane and water gas shift reactions of CO (Sasaki,

1998). However, nanowires that are confined to the channels of the mesoporous silica would be expected to be blocked from interacting with the gas phase.

2.4 Stability of Nanowires

Pt nanowires are more thermally stable when embedded inside of a silica framework(Ryoo, 2000). Pt nanowires confined to the mesopores of MCM-41 remained stable and unchanged up to temperatures of 500°C. But those wires removed by dissolving the silica in HF remained stable only up to 300°C, and broke down completely below 400°C. Those wires removed by dissolving the silica in HF were observed to have good crystallinity with diameters of 3 nm, thus the wires could be considered as single crystals.

Pt crystallite sintering behavior has been extensively studied. Various parameters have been manipulated, such as support composition, particle size and atmospheric dependence. Chen and Schmidt show that the crystallite growth rate is higher for sintering in air than in nitrogen (Chen, 1978). They attribute this to the formation of volatile oxides that escape from the surface at high temperatures. From their work, it is clear that particle growth occurs by atom diffusion rather than particle migration (Dorling, 1978). Dorling and Moss show that the size of Pt crystallites supported on silica gel depends on the firing temperature; reactivity decreases with decreasing surface area (Dorling, 1966). Surface mobility is dependent on particle size and temperature in porous silica (Zhou, 1993).

2.5 Literature Applied to this Study

Using the techniques for synthesis of mesoporous silicates reported in the literature, SBA-15, MCM-41, SBA-11 and Aerosol are prepared. These mesoporous

silicates represent morphologies of one-dimensional and three-dimensional hexagonal channels. The channel diameters are uniform and in the ranges of 2 to 7 nm. Pt crystallites have been shown to be synthesized inside of these mesoporous silicates by a variety of techniques. Pt nanowires are seen to be formed by volatile Pt ionic salts during the reduction treatment. The studies reported have shown that Pt nanowires are imaged by TEM. What remains to be done are the substrate structure insensitive catalytic studies of Pt nanowires and Pt nanoparticles inside of the mesoporous. Using the techniques discussed here, the catalytic studies will be performed to determine the role of Pt and Silicate substrate morphologies and interactions in the structure insensitive reactivity of CO oxidation on Pt catalysts.

CHAPTER 3

Characterization Methods

3.1 Reference Materials

In order to establish a benchmark to compare the novel materials synthesized in this research, we used reference samples of 0.5 wt. % Pt/Al_2O_3 (Engelhard) and 1.0 wt. % Pt/SiO_2 (Aldrich). Both reference samples were received in a reduced form. These catalysts were again reduced in flowing hydrogen during chemisorption, primarily to remove atmospheric contaminants adsorbed onto the Pt surface. The reduction was at 350°C for 2 hours under flowing 100 % hydrogen gas. Following chemisorption, these samples were characterized by a number of techniques to determine their metal particle sizes and size distributions. Each of these techniques and the resulting data are presented in this chapter.

3.2 Scanning Transmission Electron Microscopy (STEM)

The JEM-2010F was used to achieve the high quality images needed for accurate particle size analysis. The JEM-2010F is a 200kV analytical TEM with an ultra high resolution pole piece equipped with an energy dispersive X-ray spectrometer (EDS). Lattice image resolution of 0.14 nm is achievable, as well as point resolution of 0.19 nm. The system is equipped with Oxord Link ISIS analytical software for EDS analysis.

STEM allows imaging of metal particles that are located within the pore structure of the oxide lattice. Resolution at high magnification clearly shows the presence of Pt metal crystallites. Sharp contrast allows for direct measurement of diameters, using Digital Micrograph Software.

Both the 0.5 wt. % Pt/Alumina and the 1.0 wt. % Pt/Silica showed numerous well defined spherical particles with excellent contrast between the substrate and the crystallites.

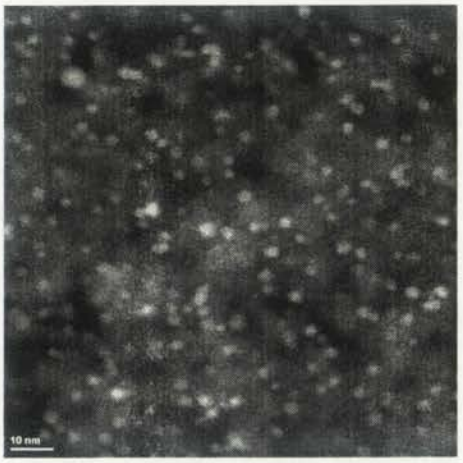

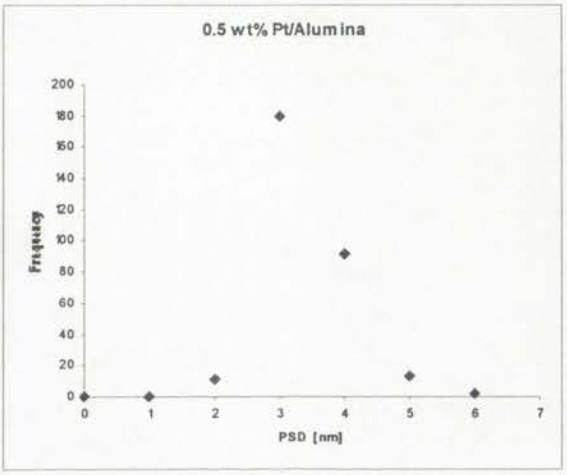

Figure 1 – STEM Image of 0.5 wt. % Pt/Alumina. The number average Average diameter is 2.9 nm from the particles size distribution.

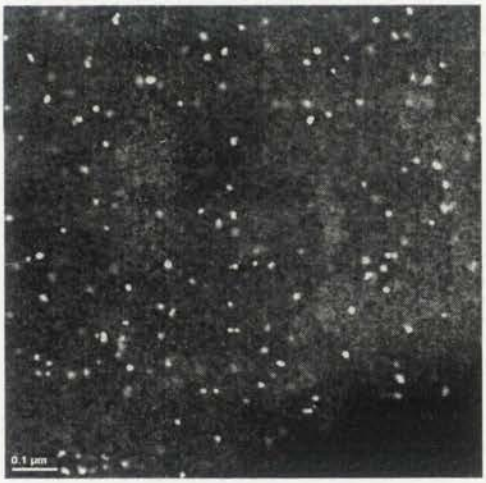

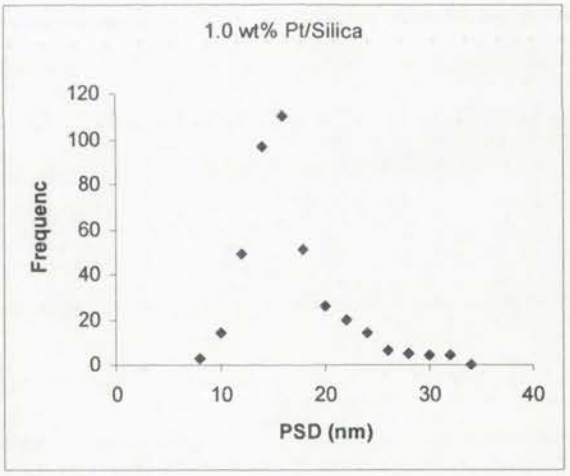

Figure 2 – STEM Image of 1.0 wt. % Pt/Silica. The number average diameter is 15.8 nm from the particles size distribution.

From the measured particle size distribution, we can calculate the number average diameter (equation 3.1), the surface average particle diameter (equation 3.2), and the volume average particle diameter (equation 3.3).

$$d_n = \frac{\sum n_i d_i}{n} \tag{3.1}$$

$$d_s = \frac{\sum n_i d_i^3}{\sum n_i d_i^2} \tag{3.2}$$

$$d_v = \frac{\sum n_i d_i^4}{\sum n_i d_i^3} \tag{3.3}$$

Where n_i is the number of particles of diameter d_i.

Sample	d_n	d_s	d_v
0.5 wt. % Pt/Alumina	2.9 nm	3.2 nm	3.3 nm
1.0 wt. % Pt/Silica	15.6 nm	21.1 nm	31.0 nm

Table 1 – Number Average Diameter (d_n), Surface average particle diameter, (d_s) Volume average Particle diameter (d_v).

3.3 X-Ray Diffraction (XRD)

XRD has the advantage in that it is non-destructive, and is a relatively simple technique to perform. Monochromatic x-rays are focused on the powder sample. The x-rays interact with the crystal lattice, and the intensity of the diffracted beam is measured as a function of angle (2θ). The fundamental equation for XRD is the Bragg's law:

$$n\lambda = 2d\sin(\theta) \tag{3.4}$$

The variables in the Bragg Equation are: n the diffraction order (an integer); λ the wavelength of x-rays; d the lattice spacing; and θ the angle between the x-ray beam and the lattice plane.

Powdered samples were analyzed by X-ray diffraction (XRD) in the XRD laboratory located in the Department of Earth and Planetary Sciences at the University of New Mexico, using a Scintag Pad V diffractometer with DataScan 4 software (from MDI, Inc.) for system automation and data collection. Cu-K-alpha radiation (40 kV, 35 mA) was used with a Bicron Scintillation detector (with a pyrolitic graphite curved crystal monochromator). Data were analyzed with Jade 6.5 Software (from MDI, Inc.) using the ICDD (International Center for Diffraction Data) PDF2 database (rev. 2004) for phase identification.

The measurement of average crystallite size is possible by XRD in conjunction with the Scherrer Formula. The Scherrer formula uses the observed line broadening to determine the average particle size. X-ray line broadening results from instrumental imperfections, finite crystal size, and crystal strain. After subtracting the background, the full-width-half-max (FWHM) value of the Pt(111) peak can be used in the Scherrer

formula to derive an average crystal size. In calculating FWHM, the instrumental contribution to line broadening is first determined by using a sample of corundum with large crystallites (and hence negligible line broadening). The instrumental contribution is subtracted before applying the Scherrer equation to determine mean crystallite size.

$$t_{crystal} = \left(\frac{4}{3}\right)\frac{k\lambda}{(FWHM)Cos(\theta)} \tag{3.5}$$

The variables of the Scherrer formula are: k the shape factor (approximately 0.9); λ the wavelength of the radiation; ($FWHM$) the measurement of line breadth at half maximum intensity in radians; and θ the angle of diffraction. The factor (4/3) accounts for the spherical shape of the metal crystallites.

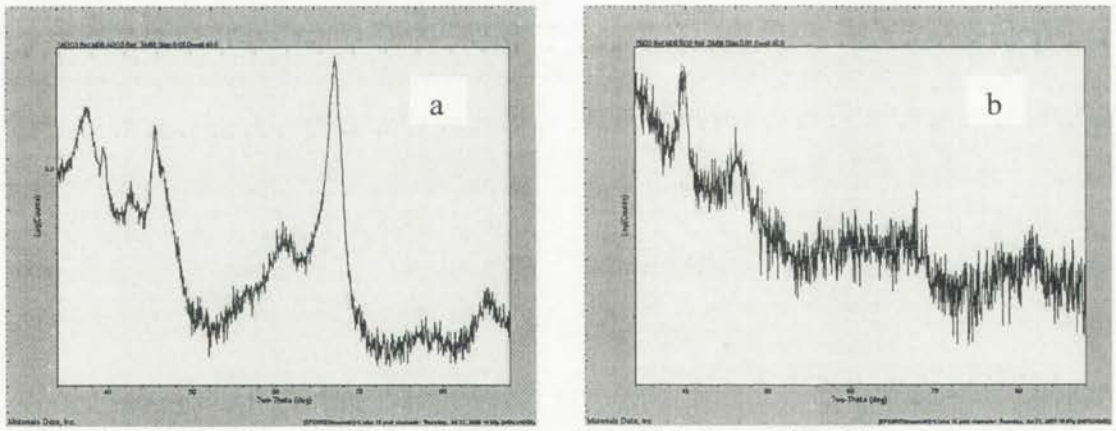

Figure 3 – XRD Plots: a) 0.5 wt. % Pt/Alumina; b) 1.0 wt. % Pt/Silica.

XRD scattering data were measured for both reference samples, however, only data from the 1.0 wt. % Pt/Silica could be used. The low weight loading of Pt, for the 0.5 wt. % Pt/alumina reference, caused the Pt peak to be too small to be detected. The peaks seen in Fig. 3a come from the alumina. The Pt crystallite size of the 1.0 wt. % Pt/Silica sample was calculated using the Scherrer formula to be 12.4 nm.

3.4 Chemisorption

Chemisorption is based on gas molecules selectively adsorbed on surface atoms. Direct measurement of the number of active surface sites is possible because only one molecule at a time can occupy a site. The fraction of the sites occupied is directly related to the pressure and the temperature.

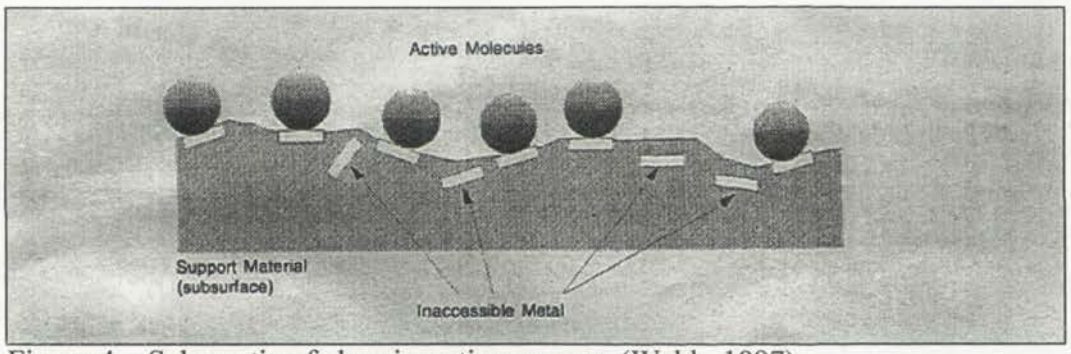

Figure 4 – Schematic of chemisorption process (Webb, 1997).

Hydrogen chemisorption data was collected using the Micromeritics 2910 pulse instrument. CO chemisorption data was collected using the Micromeritics ASAP2010 static volumetric adsorption instrument. Both instruments provide information on chemisorption uptake but differ in their approach, the former uses a flowing gas stream while the latter uses equilibrium pressure to determine the number of moles adsorbed. In the case of H_2 gas, one molecule of gas will interact with two Pt surface sites. In the case of CO gas, one molecule of gas will interact with one Pt surface site through the C atom.

Chemisorption measures directly the cumulative volume of analysis gas adsorbed. Knowing the loading of the sample and the volume of adsorbed gas allows for calculation of percent metal dispersion (γ). Percent metal dispersion is the ratio of number of accessible active sites (N_s) to the number of total atoms (N_T).

$$\gamma\% = \frac{N_s}{N_T} * 100 \tag{3.6}$$

where,

$$N_s = \frac{V_m N_A F_s}{V_{mol}} \tag{3.7}$$

The variables in the equation above are: V_m,the monolayer volume obtained as the cumulative volume adsorbed; F_s the stoichiometry factor, two for hydrogen , and one for carbon monoxide; V_{mol} the molar volume of the adsorbate at the sample temperature; the constant N_A, Avogadro's number.

Two types of chemisorption experiments are possible: static volumetric, and pulse chemisorption. In both cases, chemical adsorption occurs when vapor molecules, atoms, radicals, or ions form a direct chemical bond with active metal sites.

3.4.1 Static Volumetric Chemisorption

The static volumetric technique, using the Micromeritics ASAP2010 instrument, determines the amount adsorbed by recording the pressure after exposing the sample to precise doses of the analysis gas. The sample is outgassed at low pressure and treated with hydrogen first to ensure a clean surface before introducing the analysis gas. The

chemisorption isotherm obtained describes the variation of adsorbed gas quantity as a function of the pressure at equilibrium and at constant temperature.

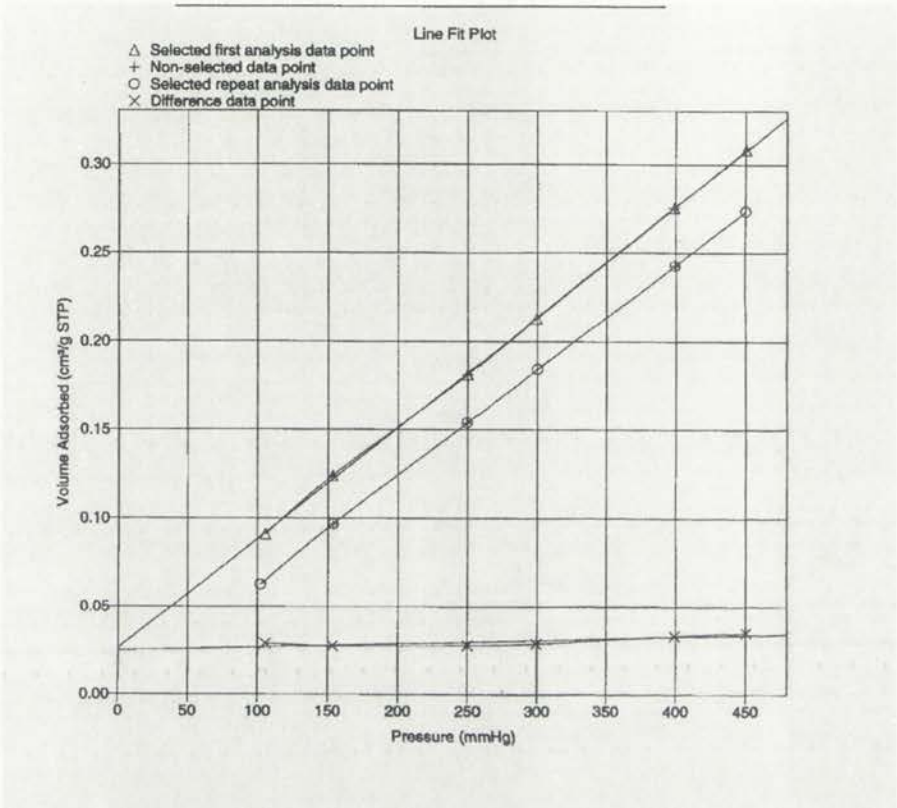

Figure 5 – Report of CO adsorption on 1.0 wt % Pt/Silica performed by static volumetric chemisorption.

The static volumetric isotherm is expressed in terms of quantity gas adsorbed vs. absolute pressure. The technique yields an experimental adsorption isotherm that involves a combination of physisorption and chemisorption. To differentiate the chemisorption from the physisorption contribution, the sample is evacuated after completion of the initial analysis which removes only the reversibly adsorbed gas. The analysis is repeated under the same conditions as the original analysis, but during the second analysis the active area of the sample is already saturated with chemisorbed molecules. The adsorbed volume of the first isotherm is a combination of the physical

and chemical adsorption. The second isotherm is the result of the repeat analysis where only reversible physisorption occurs. The difference of these two isotherms is the quantity of gas irreversibly adsorbed by the sample. A second approach to determine the chemisorbed volume is to extrapolate the first isotherm to zero pressure.

3.4.2 Dynamic Chemisorption

The dynamic pulse chemisorption analysis is done with the Micromeritics 2910 instrument. The H_2 analysis gas is routed through the sample and to a TCD detector, in which argon is used as both the carrier and reference gas. H_2 uptake is measured from a series of successive injections over the sample.

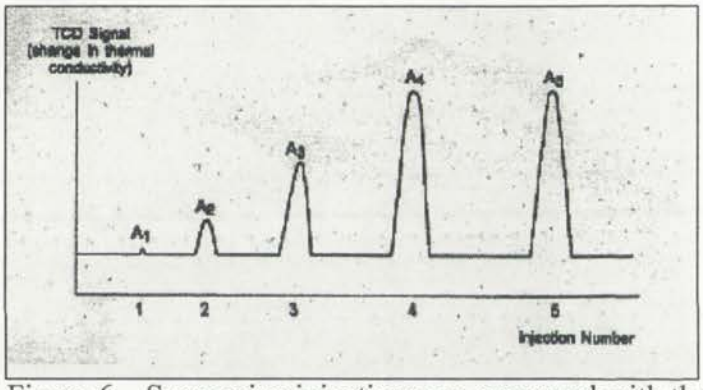

Figure 6 – Successive injections are measured with the TCD detector. Initially, the peak is small due to greater H_2 uptake. Peaks 4 and 5 show no H_2 uptake (Webb, 1997).

The analyzer consists basically of a gas inlet manifold, a flow control device, a loop arrangement by means of which active gas is injected into the carrier gas stream, a heated sample holder, a flow meter, and a detector.

The volume of the injected loop is established prior to an analysis. This is achieved by first flowing the carrier gas (argon) through the system while the detector is adjusted for zero output. Then a precise quantity of calibration gas is injected into the carrier gas stream. The calibration gas is carried through the detector producing a peak of area A. Next the loop is filled with the calibration gas and rotated into the carrier stream,

where its contents are swept to the detector. The area of the detected peak is proportional to the loop volume.

The sample is brought to analysis temperature, carrier gas flow rate is established, and the injection loop filled with analysis gas in preparation for injection. The loop valve is turned from load to inject, and the first injected volume of active gas is swept through the sample bed by the carrier gas. The loop volume should be sufficiently small so that at least five injections are totally adsorbed in order to maximize volume resolution. The total number of injections and the peak area of each injection are recorded.

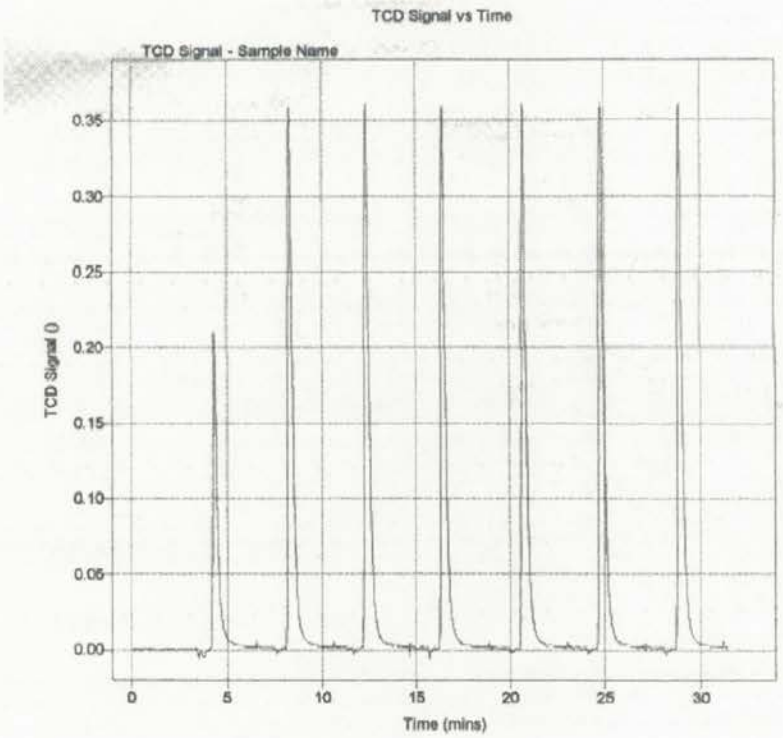

Figure 7 – Pulsed chemisorption reading of 0.5 wt. % Pt/Silica. Using 10 % Hydrogen in Argon, the Pt is seen to almost become completely saturated following the first pulsed injection.

The test is terminated when an increase in peak area can no longer be detected.

This indicates that the sample is saturated and that no more gas is being adsorbed. The peak area value displayed by the detector readout upon sample saturation corresponds to loop volume. Peak areas recorded prior to saturation indicate the proportion of the loop volume which was not adsorbed and passed through the detector. The total quantity adsorbed is the total quantity injected minus the sum of the detected amounts which passed through unabsorbed.

3.4.3 Chemisorption Results

Sample	Cumulative Volume of H_2 Adsorbed [ml/g STP]	Metal Dispersion by H_2	Cumulative Volume of CO Adsorbed [cm^3/g STP]	Metal Dispersion by CO
0.5 wt. % Pt/Alumina	0.127	44.3 %	0.236	41.03 %
1.0 wt. % Pt/Silica	0.035	6.13 %	0.0176	1.53 %

Table 2 – Chemisorption results: H_2 with static volumetric chemisorption, and CO with dynamic pulse chemisorption.

a) % Metal Dispersion, the percent active area available for interaction with the adsorbent, is calculated as follows:

$$D = \frac{N_S}{N_T} = \frac{6(v_m / a_m)}{d_{VA}} \tag{3.8}$$

b) Volume occupied by an atom in the bulk of the metal:

$$v_m = \frac{M}{\rho N_A} \tag{3.9}$$

c) Relationship between specific surface area and dispersion:

$$S_{sp} = a_m \left(\frac{N}{M} \right) D \tag{3.10}$$

d) The relationship between specific surface area and mean particle size, with units expressed in m^2/g, where d_s is expressed in nm and ρ in cm^{-1}:

$$S_{sp} = \frac{\sum n_i A_i}{\rho \sum n_i V_i} = \left(\frac{6}{\rho} \right) \frac{\sum n_i d_i^2}{\sum n_i d_i^3} = \frac{6}{\rho d_s} * 1000 \tag{3.11}$$

e) The surface average diameter:

$$d_s = 6 \left(\frac{\sum n_i V_i}{\sum n_i A_i} \right) = 6 \left(\frac{v_m N_T}{a_m N_S} \right) \tag{3.12}$$

f) Calculation of particle size from equation (3.11) with H_2 dynamic dispersion results:

0.5 wt. % Pt/Alumina (D=0.443) using

$$d_s = \frac{6 * (v_m / a_m)}{D} = \frac{6 * (15.1/8.07)}{0.443} = 25 \text{ Å} \tag{3.13}$$

1.0 wt. % Pt/Silica (D=0.061):

$$d_s = \frac{6 * (v_m / a_m)}{D} = \frac{6 * (15.1/8.07)}{0.061} = 184 \text{ Å} \tag{3.14}$$

Sample	Particle Size from H2 Chemisorption Results	Particle Size from CO Chemisorption Results	XRD	STEM
0.5 wt. % Pt/Alumina	2.5 nm	2.7 nm	n/a	2.9 nm
1.0 wt. % Pt/Silica	18.4 nm	73.3 nm	12.4 nm	15.6 nm

Table 3 – Results of particle size determined from chemisorption, XRD, and STEM.

3.4.4 Nomenclature For This Chapter

Symbol	Title	Value	Units
A_i	Area of i^{th} molecule		
a_m	Surface area per atom	8.05	Å^2
D	Metallic dispersion corresponding (V_a=5 nm)*	0.22	
d_{va}	Mean particle diameter		
n_s	Number of surface atoms (V_a=5 nm)*	$1.24 * 10^{-19}$	
ν_m	Area occupied by a Pt surface tom	8.07	Å^2
M	Atomic mass of Pt atom	195.08	g/mol
N_A	Avogadro's number	$6.03 * 10^{23}$	molecules/mol
S_{sp}	Specific surface area corresponding to (V_a=5 nm)*	55.9	m^2/g
V	Volume of adsorbed gas from chemisorptoin	(Table 2)	
V_i	Volume of i^{th} molecule		
ν_m	Volume occupied by an atom in bulk metal	15.1	Å^3
ρ	Mass density of Pt	21.45	g/cm^3
N_t	Total number of atoms		
N_s	Total number of surface atoms		

Note: * V_a=5 nm denotes hypothetical Pt crystallite of octahedron morphology with fcc (111), (110), and (100) crystal lattice structure.

3.5 CO Oxidation Rate

CO Oxidation is performed with stoichiometric CO to O_2 ratio, using a balance of He, set to a total combined flow of 100 sccm at atmospheric pressure. The reaction stoichiometry is:

$$\frac{1}{2}O_2 + CO \rightarrow CO_2 \tag{3.15}$$

CO_2, O_2, and CO effluent gases are measured using a Varian GC 3400 gas chromatograph. The instrument is inline with the flowing analysis gas directed to pass through the catalyst sample contained in a ¼ in glass plug flow reactor. A precise quantity of catalyst is loaded into the sample holder. A thermocouple is placed immediately above the powder, and the temperature is controlled to within 1°C with controlled ramps between each analysis temperature. The heating mantle is controlled with a Fuji VX temperature controller. The reactant gases were UHP 5% CO in He, 2 %O_2 in He, and a carrier gas of He. Flows were controlled by mass flow controllers. These gases were mixed together to yield an inlet gas composition of: 1% CO, 0.5% O_2, and 98.5% He.

Calibration to determine % CO in the feed gas (5% CO/He UHP), required a calibration of the supply gas. This was performed by varying the %CO in a mixture derived from 100% CO and 100% He. Varying the % CO using control flow meters upstream from the GC we could determine as area of the peak, the GC response divided by the % CO in the flow.

The GC relative response for CO and CO_2 was next determined by measuring the area of the CO and CO_2 peaks at 0 % and 100 % conversion respectively. Using this

relative response factor, the % conversion at each temperature could be measured. The rate of reaction is determined using the equation:

$$\frac{mmol\ CO_2}{g\ cat * Sec} = \frac{P}{RT} v * \frac{1}{m_{cat}} * 10^{-6} \qquad (3.16)$$

The variables are: P pressure, R ideal gas constant, T temperature, v molar flow rate, and m_{cat} mass of cataysis

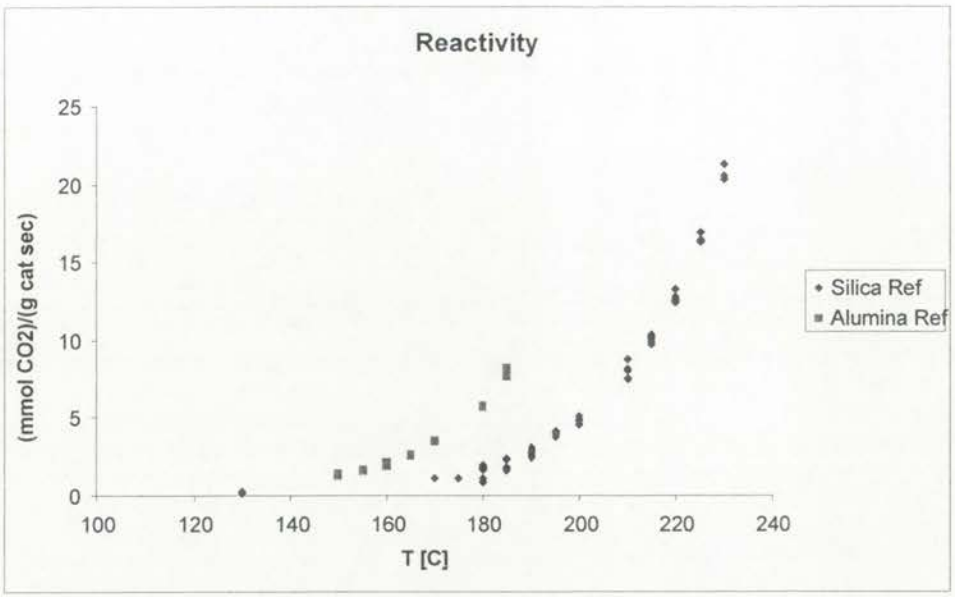

FIGURE 8 – Reactivity data of 0.5 wt. % Pt/Alumina and 1.0 wt. % Pt/Silica Reference sample. Plot of y-axis is mmol CO_2 effluent per gram catalysts second. x-axis is temperature in °C.

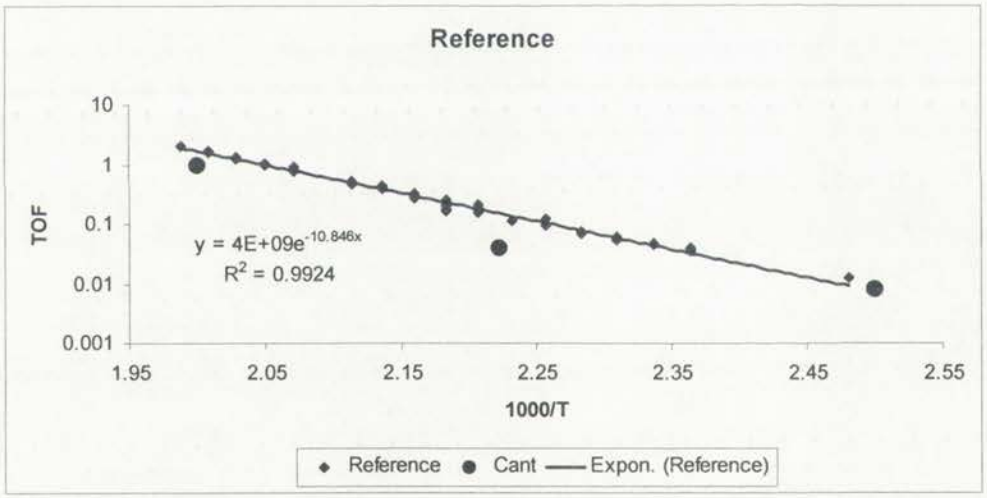

FIGURE 9 – TOF of both reference catalysts compared with the literature data from the work of Cant et. al. (Cant, 1978).

The rate of reaction can be converted to a turnover frequency (TOF) which is the moles of CO_2 formed per mole of surface Pt per second. TOF is measured in units of reciprocal seconds. It is independent of the mass, dispersion, and wt. % loading of catalyst if the reaction is structure insensitive. The TOF is determined by taking:

$$\left[\frac{mol\,CO_2}{g\ cat * \sec}\right] \div \left[\frac{Pt\ active\ surface\ sites}{g\ cat}\right] \tag{3.17}$$

Since TOF is an intrinsic value, it is possible to use the TOF to compare the reference catalysts with data presented by other researchers in the literature. The value of TOF for the reference catalysts shows very good agreement despite large differences in metal particle size and loading, confirms that the CO oxidation is structure insensitive.

The literature TOF values were obtained from a paper published by Cant N.W. et. al. (Cant, 1978). The TOF measured by the authors for the 5 wt. % Pt/Silica are shown in Figure 8 for comparison. The CO oxidation data in that study was collected with 10 Torr partial pressure of CO and 5 Torr partial pressure of O_2. The experiments reported here were obtained using 6.3 Torr CO and 3.15 Torr O_2. CO oxidation is known to be unaffected by total pressure (Boudart, 1995).

3.6 Particle size and exposed metal surface

The methods of analysis outlined in this chapter provide the information for determining crystallite size and ratio of Pt surface sites to total metal atoms. STEM allows for the direct measurement of Pt crystallites using Digital Micrograph imaging software. The XRD provides a method for measuring average crystallite size. The hydrogen and CO chemisorption uptakes provide a direct measure of the number of

exposed Pt atoms. The chemisorption gas uptake can also be used to generate estimates of crystallite size from the known surface area of the metal and the area occupied per exposed atom for the given structure. The surface area per metal atom is obtained by assuming that the exposed lattice planes consist of the fcc (111) (110) and (100) planes of a fcc cuboctahedron.

The number average diameter for the 0.5 wt. % Pt/Alumina was measured as 2.9 nm by STEM. The XRD pattern was unable to be used for this sample, since the Pt (111) peak was not distinguishable from the alumina XRD pattern. The high dispersion of this sample, and the small particle size also affected the XRD. Crystallite sizes of 2.9 nm are on the lower bound of what is measurable using the XRD and the Scherrer formula. The number average diameter agreed with that measured by both H_2 chemisorption (2.5 nm) and CO chemisorption uptake (2.7 nm).

The number average diameter for the 1.0 wt. % Pt/Silica was measured as 15.8 nm with STEM. The XRD pattern of the Pt (111) peaks indicated the Pt crystallite size average was 16.5 nm. Therefore the XRD pattern and the Scherrer formula provide diameters for 1.0 wt. % Pt/silica on the same order as those determined by % dispersion obtained from H_2 chemisorption. The agreement with CO uptake was not as good. It appears that CO uptake underestimates dispersion, so for this study we have relied on H_2 chemisorption.

As seen from the CO oxidation, the 0.5 wt. % Pt/Alumina was more reactive despite lower metal loading. The temperature range at which the 0.5 wt. % Pt/Alumina achieved 10 % conversion is 180°C. The same conversion is achieved with 1.0 wt. % Pt/Silica at 220°C. However, once the reactivity is normalized by the H_2 uptake to get

TOF, we get similar numbers for each catalysts. Taking the TOF of each, within their respective temperature ranges of 10 % conversion, results in agreement as seen in figure 9. The TOF reported by Cant. et. al. is slightly less at the temperatures indicated. Between the previous work by Cant et. al, and the current work for this study, we see excellent agreement in TOF. It is concluded from figure 9, that the CO oxidation is a substrate structure insensitive reaction. This provides a benchmark for studying the reactivity of Pt nanowires.

CHAPTER 4

Pt Supported in MCM-41 Mesoporous Silica

4.1 MCM-41 Experimental Procedure

To synthesize the MCM-41 silica powder, the procedure outlined by Beck et. al. was used (1992). A quantity of 4.71 g CTAB was completely dissolved in 65 ml DI water by gently heating and stirring until the solution became completely clear. To this was added 6.4 ml sodium silicate, which resulted in a pH of 12. The pH was reduced to 10, by slowly adding 17.3 ml 1 N HNO_3. The slightly opaque solution was transferred to a polypropylene bottle maintained at 80°C for 6 hours. At the end of 6 hours, an orange/white precipitate had formed. The precipitate was subsequently filtered, washed with DI, and allowed to dry in air at room temperature. The powder was calcined in air at 500°C for 12 hours, with a ramp rate 5°C/min. The BET surface area analysis of the MCM-41 powder was measured to be 1059.6 m^2/g.

Pt anionic crystalline salts were embedded into the mesoporous silica by wet impregnation. 2.0 g MCM-41 was suspended into 300 ml DI with vigorous stirring at room temperature. To this solution was added 218 mg $H_2PtCl_6*6H_2O$ to form a yellow solution. The sample was allowed to stir for an additional 24 hours before being transferred to vacuum to completely dry to a fine yellow powder. This powder was collected and dried under vacuum for an additional 24 hours before being separated into equal halves to be reduced under wet and dry reductions. A loading of Pt of 5 wt. % was achieved by the incipient wetness method. The reduced samples were then characterized by STEM, XRD, Chemisorption, and CO oxidation.

It was found that in order to minimize the formation of Pt nanowires, it was necessary to calcine the dry reduced sample prior to the reduction. The calcination procedure involved heating the sample to 150°C for 2 hours with a ramp rate of 0.73°C/min.

4.2 MCM-41 STEM Results

STEM images confirmed that following wet reduction, the vast majority of the Pt formed nanowires within the mesoporous silica channels. In the case of dry reduction, the majority of the Pt formed well dispersed metal crystallites throughout the silica powder. STEM images indicate that the nanowires conform to the shape of the mesoporous channels of MCM-14. Diameters measured from STEM images are of 2.7 nm, consistent with the pore diameter of MCM-41 silica. Nanoparticle particles measured with STEM are in the ranges of 1.7 to 2.7 nm.

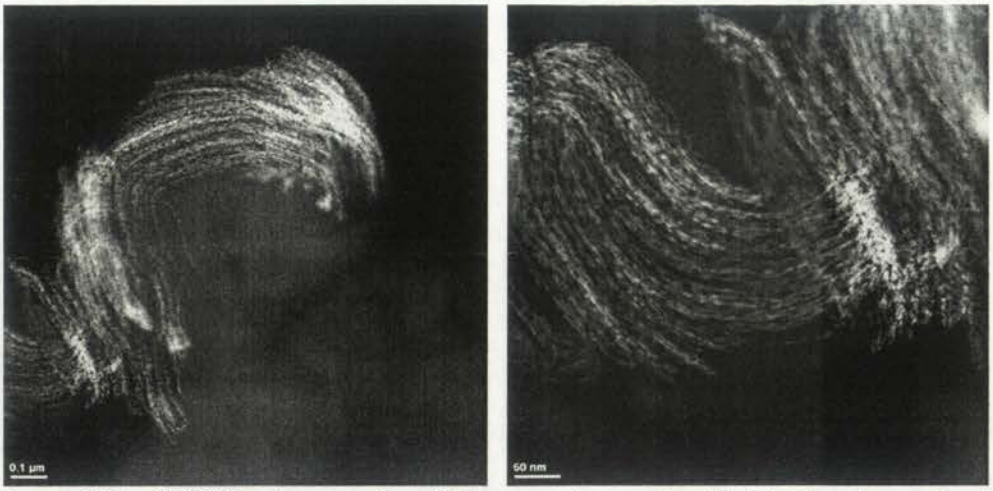

Figure 10 – STEM micrographs of Pt nanowires embedded in the channels of 5.0 wt. % Pt/MCM-41 following wet reduction.

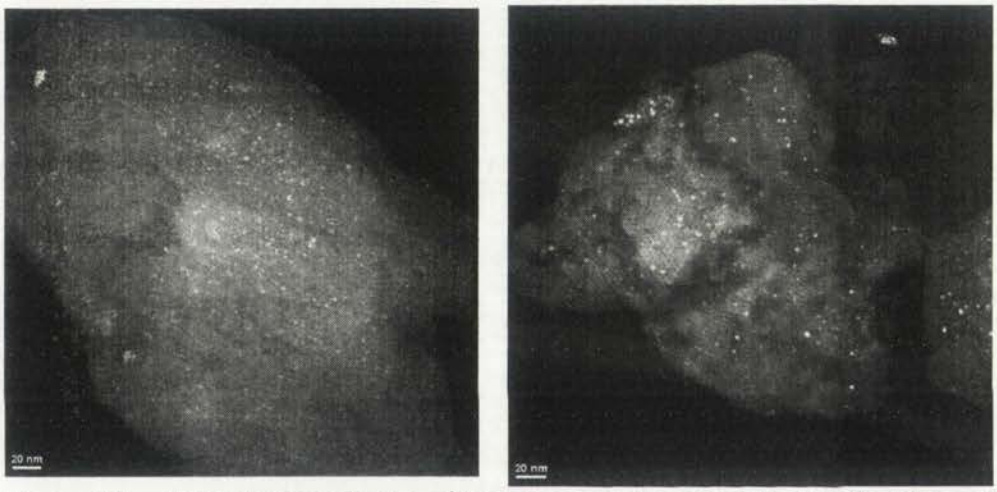

Figure 11 – STEM micrographs of Pt nanoparticles embedded in the channels of 5.0 wt. % Pt/MCM-41 following wet reduction.

4.3 MCM-41 Chemisorption Results

Sample	Reduction	Cumulative Volume Adsorbed [H_2 ml/g STP]	% Metal Dispersion	Mean Particle Size
5 wt. % Pt/MCM-41	Wet	0.768	26.8	4.2 nm
5 wt. % Pt/MCM-41	Dry	1.49	51.9	2.2 nm

Table 4 – Results of H_2 Dynamic Chemisorption and eq. 3.12.

Sample	Reduction	Cumulative Volume Adsorbed [CO cm^3/g STP]	% Metal Dispersion	Mean Particle Size
5 wt. % Pt/MCM-41	Wet	1.29	22.5	5.0 nm

Table 5 – Results of CO Static Volumetric Chemisorption and eq. 3.12.

Sample	Reduction	Cumulative Volume Adsorbed [CO cm^3/g STP]	% Metal Dispersion	Mean Particle Size
5 wt. % Pt/MCM-41	Dry	2.03	35.3	3.2 nm

Table 6 – Results of CO Static Volumetric Chemisorption and eq. 3.12.

4.4 MCM-41 XRD Results

Sample	Reduction	XRD Average Particle Size
5 wt. % Pt/MCM-41	Wet	4.8 nm
5 wt. % Pt/MCM-41	Dry	4.2 nm

Table 7 – Results of XRD and Scherrer Forumla.

4.5 MCM-41 CO Oxidation TOF Results

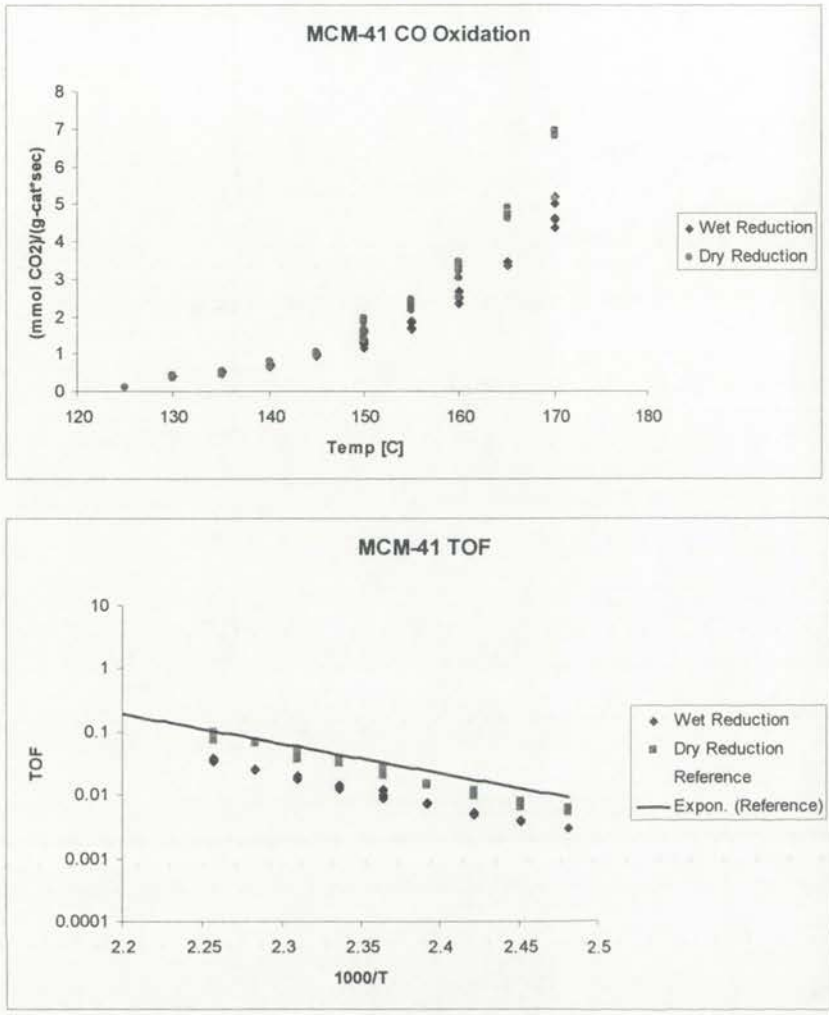

Figure 12 – CO oxidation reactivity data for 5 wt. % Pt/MCM-41, and Arrhenius plot for TOF compared with the reference Pt sample.

4.6 MCM-41 Experimental Conclusions

STEM provides details of crystallite and mesopore morphology. The pore diameter for MCM-41 is 2.7 nm (Beck, 1992). Following wet reduction, Pt agglomerates into localized regions. These regions of high loading are predominately occupied with nanowires, with very few nanoparticles interspersed. Nanowires appear to be discontinuous and comprised of closely spaced elongated nanoparticles. These nanowires have intermittent voids along the path of the mesopores. Following dry

reduction, the Pt particles are dispersed throughout the silica powder. In most cases, the nanoparticles are of the same size as the channel diameters, and they predominately reside inside of the channels

Accessibility of nanowires and nanoparticles to CO oxidation are similar. The reactivity enables us to conclude that CO is accessible to both nanowires and nanoparticles. The nanosized cuboctahedron shape assumed to be spherical in the reference samples apply to the Pt crystallites in MCM-41. Particle size determined by XRD, H_2 chemisorption, and STEM give similar results even though the geometric shape factor for each is different. Nanoparticles will tend to have a higher surface to bulk ratio than nanowires, which would lead to greater chemisorption. A comparison between XRD line broadening indicates similar morphologies between the nanoparticles and the nanowires.

CHAPTER 5

Pt Supported in SBA-15 Mesoporous Silica

5.1 SBA-15 Experimental Procedure

A mass of 4.02 g P123 (aldrich) was dissolved into a solution of 30 ml DI and 120 ml 2 M HCl. The P123 was stirred into solution for 2 hours before completely dissolving at room temperature. The solution was clear with a slight layer of white foam on the surface. To the solution was added 9.4 ml TEOS, and this was vigorously mixed for an additional 3 minutes. The solution became slightly white and opaque and was transferred to a polypropylene (PP) bottle maintained at 38°C without stirring. After 20 hours, a white precipitate had formed at the bottom of the PP bottle. This was filtered, washed with DI, and allowed to dry in air for 4 hours. The powder was then calcined in air at 500°C for 12 hours with a ramp rate of 5°C/min. Following calcination, the BET surface area was measured to be 856.2 m^2/g.

For the impregnation of Pt into the silica SBA-15 powder, 2.0 g SBA-15 powder was suspended into 300 ml DI at room temperature by vigorously stirring. To this was added 297 mg of $H_2PtCl_6*6H_2O$, which immediately dissolved to form a yellow solution. This mixture was allowed to continue stirring for an additional 24 hours before being transferred to vacuum. Under vacuum, the solution was evaporated to complete dryness, and the yellow/white powder was collected. This powder was dried under vacuum for an additional 24 hours before being separated into equal halves for wet and dry reduction. A loading of Pt of 6.6 wt. % was achieved by the impregnation method.

For both reductions, the tube furnace was ramped at 0.73°C/min to 200°C, which was maintained for 2 hours. In the case of the dry reduction, 100% hydrogen gas at 50

sccm was passed over the sample. For wet reduction, the hydrogen gas was bubbled through DI to saturate before being introduced to the sample chamber.

5.2 SBA-15 STEM Results

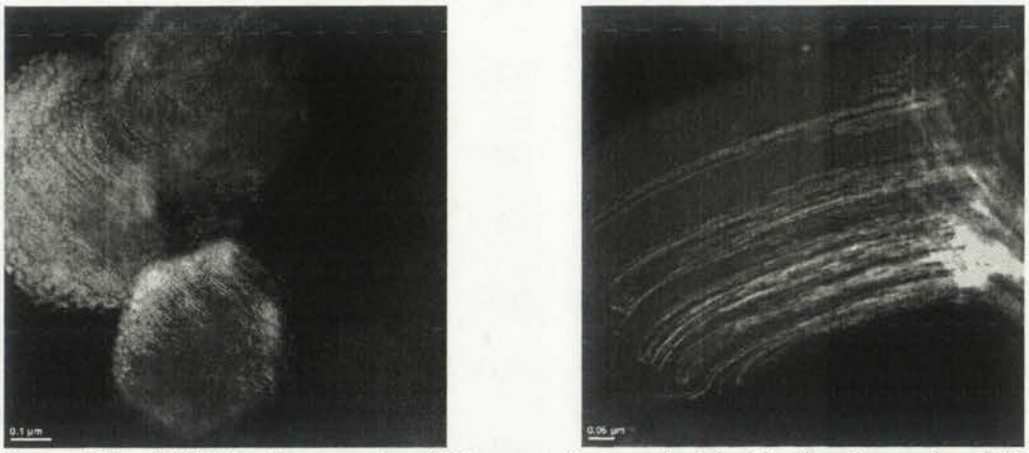

Figure 13 – STEM micrographs of Pt nanowires embedded in the channels of SBA-15 following wet reduction.

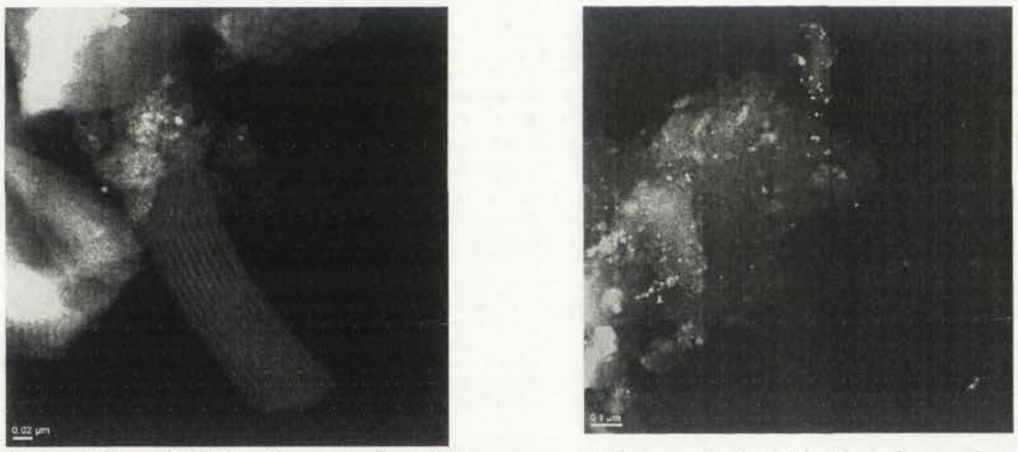

Figure 14 – STEM micrographs of Pt nanoparticles embedded in the channels of SBA-15 following dry reduction.

5.3 SBA-15 Chemisorption Results

Sample	Reduction	Cumulative Volume Adsorbed [H_2 ml/g STP]	% Metal Dispersion	Mean Particle Size
6.6 wt. % Pt/SBA-15	Wet	0.473	12.5	9.0 nm
6.6 wt. % Pt/SBA-15	Dry	0.542	14.3	8.0 nm

Table 8 – Results of H_2 Dynamic Chemisorption and eq. 3.12.

5.4 SBA-15 XRD Results

Sample	Reduction	XRD Average Particle Size
6.6 wt. % Pt/SBA-15	Wet	7.6 nm
6.6 wt. % Pt/SBA-15	Dry	6.4 nm

Table 9 – Results of XRD and Scherrer Formula.

5.5 SBA-15 CO oxidation and TOF Results

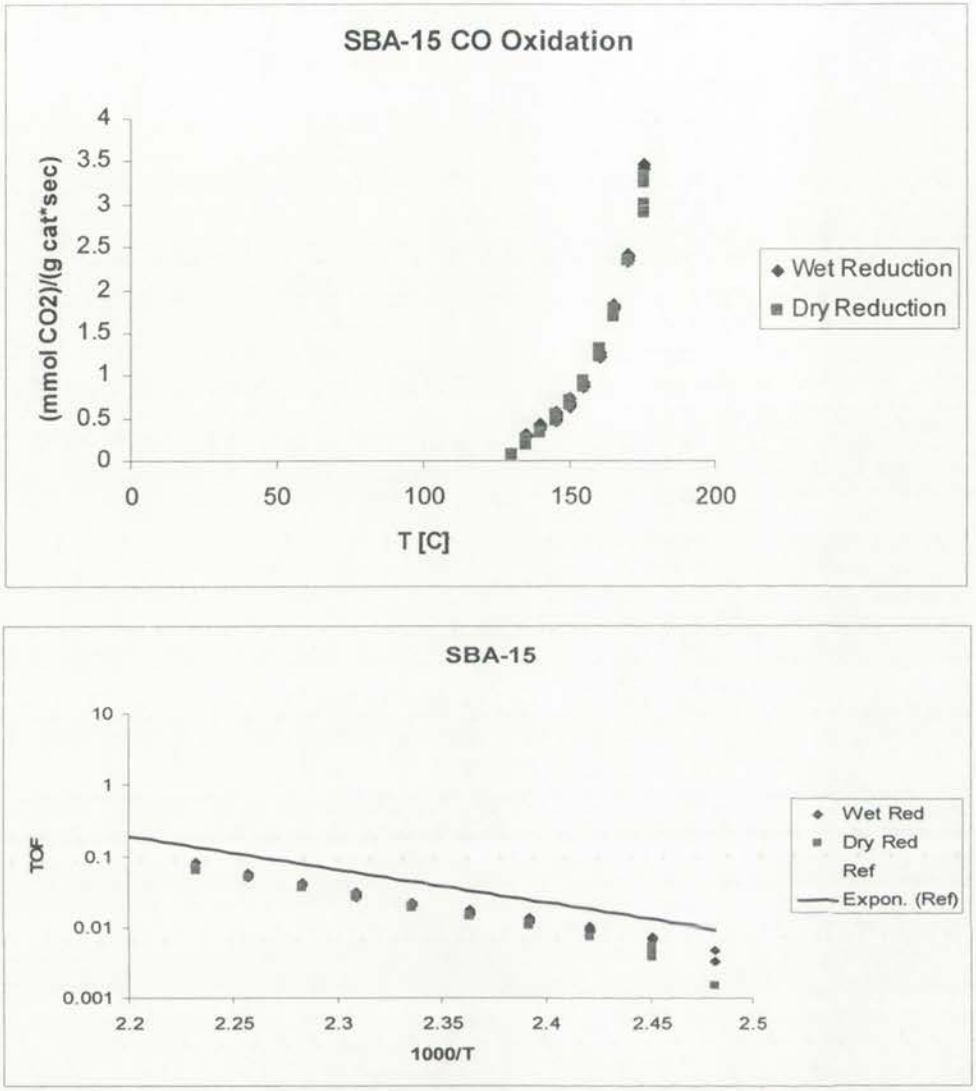

Figure 15 – CO oxidation reactivity data of 6.6 wt. % Pt/SBA-15, and the Arrhenius plot of reactivity for the reference catalysts is also shown.

5.6 SBA-15 Experimental Conclusion

STEM images show that nanowires form in localized regions when wet reduction is used. In the case of dry reduction, the nanoparticles are more prevalent and more uniformly dispersed. STEM of both samples provide evidence that the nanowires and nanoparticle conform to the pore diameters of SBA-15. The pore diameter measured

from Pt nanowires indicated they were roughly 7 nm. Dynamic H_2 chemisorption and XRD provides average size distributions that agree within 1 nm.

The relatively large pore diameter of SBA-15 provides paths for Pt migration during impregnation and reduction. The larger pore structure does not hinder the CO oxidation or the chemisorption uptake. Mean particle sizes determined from chemisorption and XRD all agree within 2.6 nm. This is attributed to the case where some nanowires formed during dry reduction. In addition, some nanowires are formed due to adsorbed moisture available to the Pt during the dry reduction.

Chapter 6

Pt Supported in SBA-11 Mesoporous Silica

6.1 SBA-11 Experimental Procedure

Into a solution of 80 ml 2 M HCl and 20 ml DI water was completely dissolved 4.0 g Brij 56 (Aldrich). This required a number of hours before the waxy Brij 56 completely dissolved into the DI at room temperature. To this solution was added 9.4 ml TEOS to form a slightly opaque solution. This solution was mixed for a few minutes before being transferred to a PP bottle maintained at room temperature for 20 hours. Following 20 hours, a waxy phase had formed at the bottom of the PP bottle, which was filtered with DI and washed over a number of days before only a white powder remained on the filter paper. This was dried in air before being calcined. The calcination was performed in air at 500°C for 12 hours with a ramp rate of 5°C/min. The BET surface area analysis was measured to be 791.8 m^2/g.

1.63 g SBA-11 powder was suspended into 225 ml DI at room temperature with vigorous mixing. To this solution was added 0.21 g $H_2PtCl_6*6H_2O$. The solution became yellow and was allowed to mix for an additional 24 hours before being transferred to vacuum. Under vacuum the solution was evaporated to leave a fine yellow powder. The yellow powder was collected and dried under vacuum for an additonal 24 hours. The powder was divided equally for wet and dry reduction. A loading of Pt of 5.7 wt. % was achieved. Dry reduction was performed under 100 % flowing H_2 in a tube furnace at 200°C for 2 hours. The ramp rate of the furnace was 0.73°C/min. The same settings were used for the wet reduction, except that the H_2 gas was first bubbled through DI water to saturate before reducing the Pt.

6.2 SBA-11 STEM Results

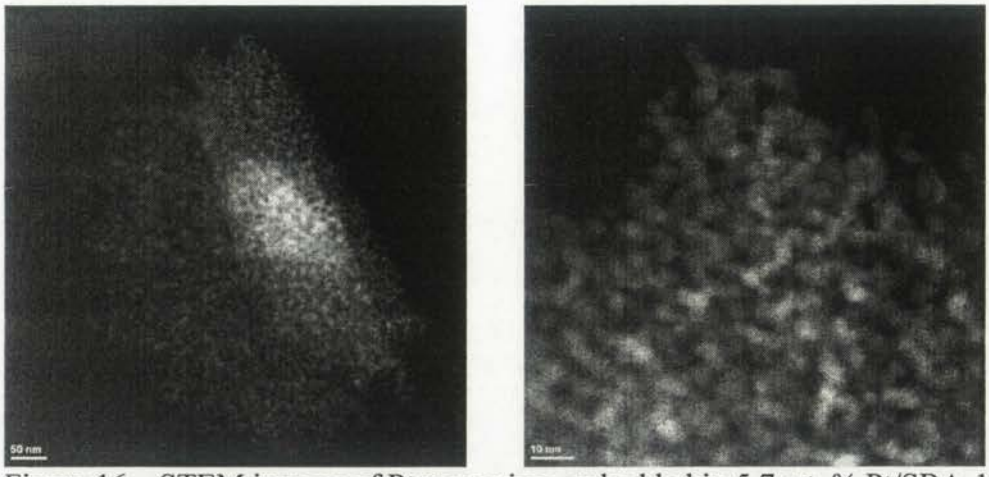

Figure 16 – STEM images of Pt nanowires embedded in 5.7 wt. % Pt/SBA-11 following wet reduction.

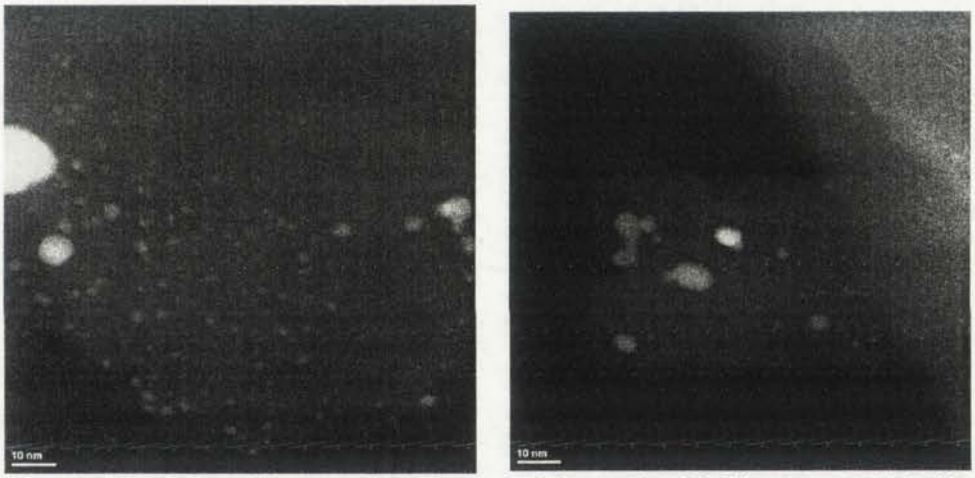

Figure 17 – STEM images of Pt nanoparticles embedded in 5.7 wt. % Pt/SBA-11 following dry reduction.

6.3 SBA-11 Chemisorption Results

Sample	Reduction	Cumulative Volume Adsorbed [H_2 ml/g STP]	% Metal Dispersion	Mean Particle Size
5.7 wt. % Pt/SBA-11	Wet	1.10	33.7	3.3 nm
5.7 wt. % Pt/SBA-11	Dry	0.439	13.4	8.4 nm

Table 10 – Results of H_2 Dynamic Chemisorption and eq. 3.12.

6.4 SBA-11 XRD Results

Sample	Reduction	XRD Average Particle Size
5.7 wt. % Pt/SBA-11	Wet	5.5 nm
5.7 wt. % Pt/SBA-11	Dry	3.7 nm

Table 11 – Results of XRD and Scherrer Formula.

6.5 SBA-11 CO Oxidation TOF Results

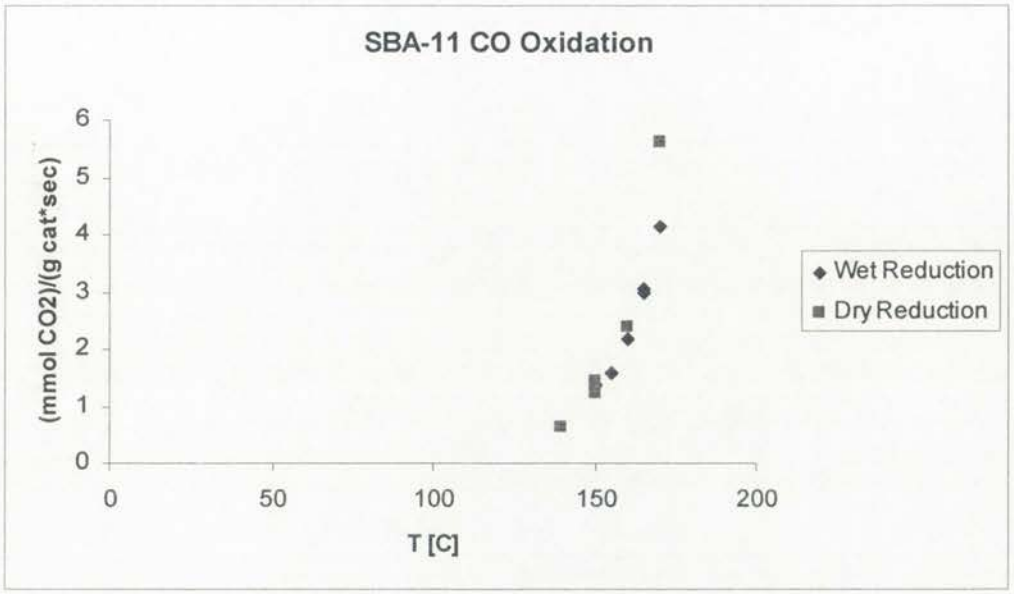

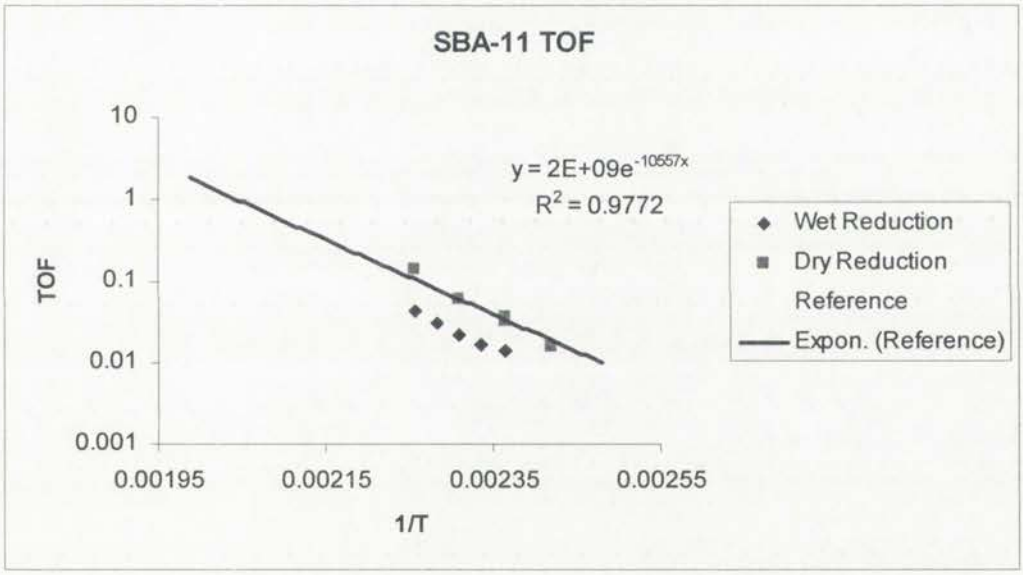

Figure 18 – CO oxidation reactivity data for 5.7 wt. % Pt/SBA-11, and Arrhenius plot for TOF compared with the reference Pt sample.

6.6 SBA-11 Experimental Conclusions

Of all the samples in this study, SBA-11 is unique in that the mesoporous channel structures are three-dimensional and intertwined. The channels cross at many places, providing better access for chemisorption and for CO oxidation. In regions where the Pt agglomerates into high concentrations following wet reduction, the Pt forms tripod like structures with multiple branches. Diameters of the Pt nanowires were measured with STEM to be roughly 2.7 nm. The mobility of the Pt nanoparticles in the open mesoporous structure tend to lead to regions of localized high concentrations. Where nanoparticles are in close proximity, they tend to agglomerate.

The chemisorption and XRD results contradict each other. Chemisorption indicates that the particles following dry reduction are over 8 nm in diameter. These size particles would not conform to the diameters of the mesoporous channels. This can be attributed to the branch structures of the Pt nanowires. This structure leaves more accessible surface area to chemisorption.

With the XRD line broadening and the Scherrer formula, the nanowires are 5.5 nm in size. The Scherrer formula is based upon the assumption that the Pt particles are spherical. Branched structures allow for particles of a variety of sizes and morphologies. It is also possible that the particles more readily agglomerate at the surface of the silica, rather than in the pores.

CHAPTER 7

Pt Supported in Aerosol Mesoporous Silica

7.1 Aerosol Experimental Procedure

A quantity of 12.5 g CTAB was completely dissolved into 250 ml DI and 5 ml of 1N HCL solution. To the clear solution was added 50 ml TEOS, which immediately became cloudy. After stirring for a few minutes, a clear solution formed. The clear solution was transferred to a sonicator bath with which to form aerosol droplets from the solution. Nitrogen gas at 5 ml/min was used to carry the vapor through a tube furnace set at 125°C. The powder was collected on a 0.2 μm filter paper. This white powder was then calcined in air at 500°C for 12 hours with a ramp rate of 5°C/min. The BET surface area was measured to be 1339.2 m^2/g.

A Pt loading of 6.2 wt. % was achieved by the incipient wetness method. 2.0 g Aerosol silica was suspended into 300 ml DI under vigorous mixing at room temperature. To the solution was added 0.2765 mg $H_2PtCl_6*6H_2O$. This was allowed to mix for 24 hours before being transferred to vacuum where the solution was evaporated to a fine yellow powder. The powder was collected and dried under vacuum for an additional 24 hours before being separated into equal halves for wet and dry reduction. Dry reduction was performed by passing a 50 sccm 100% H_2 gas over the sample loaded into a tube furnace. The furnace was set to 200°C for 2 hours with a ramp rate of 0.73°C/min. The wet reduction was performed identically, except that the H_2 gas was saturated with water by bubbling it through DI before being introduced to the sample.

7.2 Aerosol STEM Results

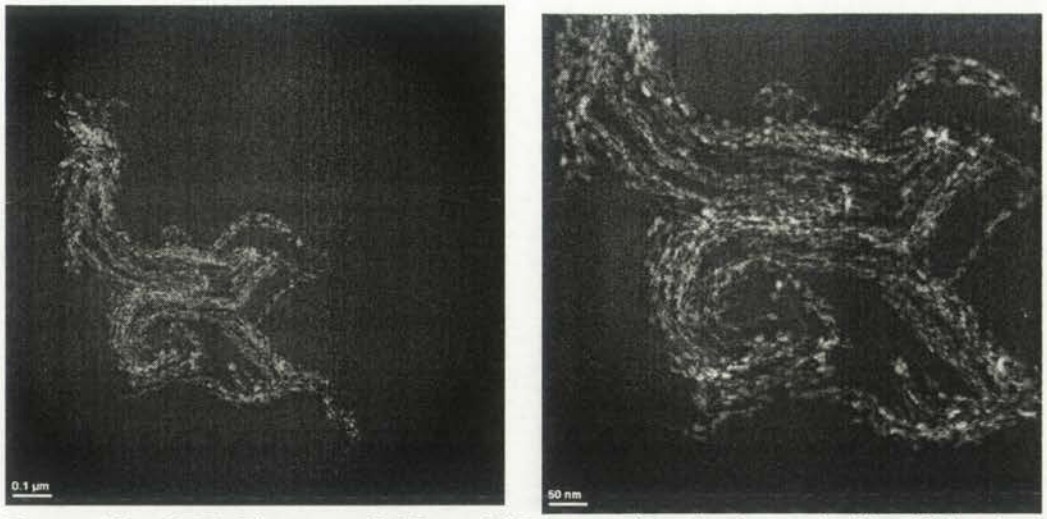

Figure 19 – STEM images of 6.2 wt. % Pt nanowires in Aerosol silica following wet reduction.

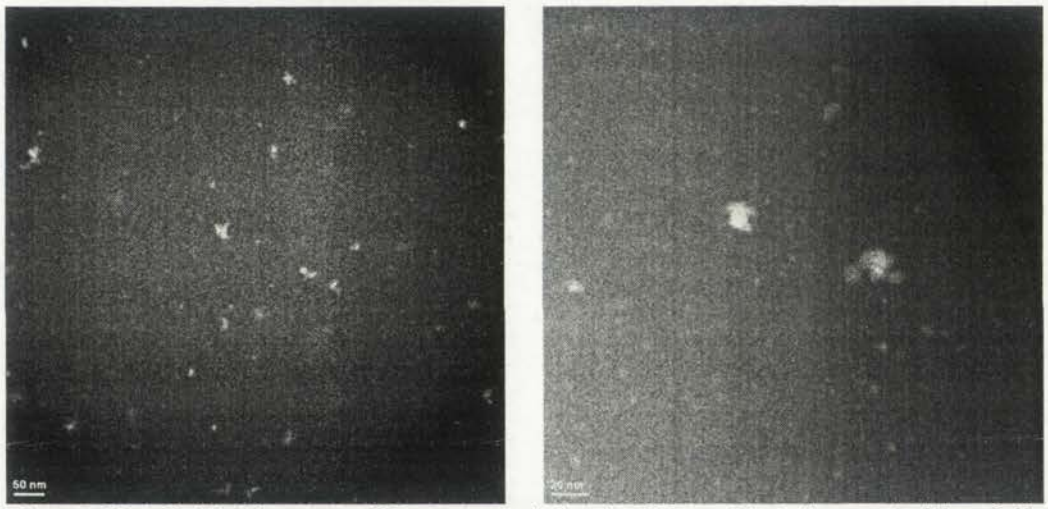

Figure 20 – STEM images of Pt nanoparticles in 6.2 wt. % Pt/Aerosol silica following dry reduction.

7.3 Aerosol Chemisorption Results

Sample	Reduction	Cumulative Volume Adsorbed [H_2 ml/g STP]	% Metal Dispersion	Mean Particle Size
6.2 wt. % Pt/Aerosol	Wet	0.579	16.3	6.9 nm
6.2 wt. % Pt/Aerosol	Dry	0.706	19.8	5.6 nm

Table 12 – Results of H_2 Dynamic Chemisorption and eq. 3.12.

7.4 Aerosol XRD Results

Sample	Reduction	XRD Average Particle Size
6.2 wt. % Pt/Aerosol	Wet	4.9 nm
6.2 wt. % Pt/Aerosol	Dry	3.6 nm

Table 13 – Results of XRD and Scherrer Formula.

7.5 Aerosol CO Oxidation and TOF Results

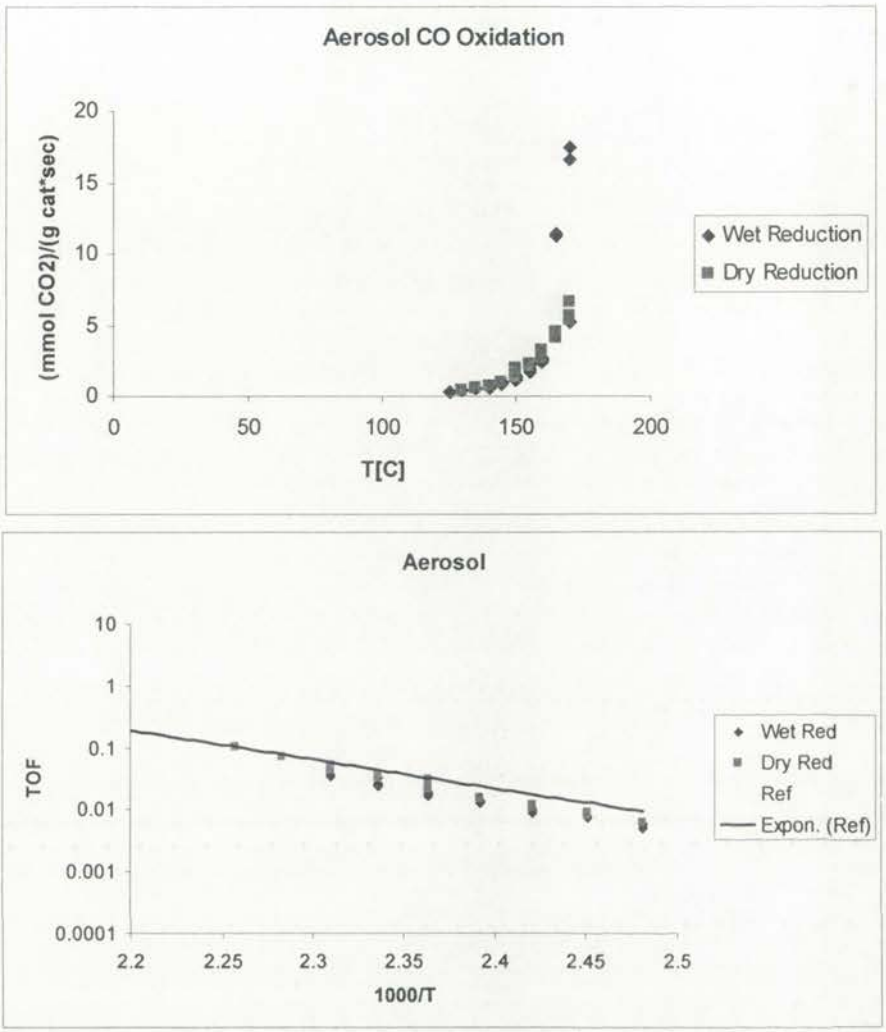

Figure 21 – CO oxidation reactivity data of 6.2 wt. % Pt/Aerosol, and the TOF data compared with the reference.

7.6 Aerosol Experimental Conclusions

Wet reduction allows the mesoporous channels to be filled with nanowires in highly localized regions. Dry reduction results predominately in particles evenly distributed throughout the aerosol powder. STEM images show nanowires filling the pores and nanoparticles conforming in size to the diameters of the mesoporous structure. However, from each reduction, there is a mix of nanowires and nanoparticles. The chemisorption uptake and XRD analysis for particle size determination differ by 2 nm in each reduction. H_2 chemisorption uptake and CO oxidation are similar between reduction techniques. Therefore, the TOF is similar. The results indicate that similar uptake suggests both nanoparticles and nanowires are similarly accessible to gas phase transport through the silica. In terms of matching the reference TOF, aerosol gave the closest agreement. The study shows that there is very little difference in the reactivity of Pt nanowires and Pt nanoparticles.

CHAPTER 8

Conclusion and Recommendations

8.1 Conclusion

My results show that mesoporous silica structures can be used as templates for the synthesis for nanowires and nanoparticles. Wet reduction leads to nanowires. In contrast, dry reduction favors the formation of nanoparticles. The nanowires take the shape of the mesopores. Both nanowires and nanoparticles are completely dispersed throughout the mesoporous silica.

Although the nanowires completely fill the pores, they are comparable to the nanoparticles in terms of CO oxidation and chemisorption accessibility. Except for SBA-11, chemisorption results are as expected; the nanoparticles have higher Pt active surface areas compared to the nanowires. The SBA-11 morphology is unique in that the mesopores are intertwined through a 3-dimensional cross section structure. The SBA-11 nanowires are presumably as accessible as the nanoparticles since they are not confined to 1-dimensional pores. It is also possible that the particles outside of the pores agglomerate more readily. In fact, they appear to be even more accessible since the nanowires have a metal dispersion value 2.5 times greater than the nanoparticles. This is in direct contradiction to the other samples studied in which the dispersion of the nanoparticles is greater than that of the nanowires.

The other silicon porous structures are 1-dimensional. Although SBA-15 and MCM-41 have the same morphology, with the exception of pore wall thickness and pore diameter, the metal dispersion of the nanoparticles is twice that of the nanowires. In SBA-15, nanoparticles and nanowires have similar values of metal dispersion, much

lower than the values from MCM-41. Aerosol has a spherical morphology, and is much like MCM-41, except that the pores follow a much more tortuous path. Perhaps this explains why the metal dispersion values are much lower than from MCM-41.

The role of mesoporous wall thickness is seen in comparing the H_2 uptake between MCM-41 and SBA-15. The MCM-41 wall thickness is much thinner than that of SBA-15. Presumably the thinner wall thickness allows for higher rates of passage of CO and H_2 uptake.

Interestingly the aerosol derived silica shares the thin walls that characterizes MCM-41. The H_2 uptake between the two is quite comparable with MCM-41 nanowire structure.

8.2 Recommendations

The procedure of developing either nanowires or nanoparticles through wet or dry reduction is not perfect. For instance, to a small extent, nanowires are seen after wet reduction and nanoparticles after dry reduction. To conclusively identify the role of morphology, improving the control over synthesis would be beneficial. New techniques for preparing exclusively each morphology are needed for this investigation. We found that calcination prior to dry reduction helps decrease the formation of nanowires to a minimum.

Since the data shows that the reactivity of Pt nanowires is comparable to Pt nanoparticles, the next step would be to investigate the differences in sintering behavior between the morphologies. We would expect that the nanowires would be more resistant to ripening and coalescence, due to their lower surface energy relative to nanoparticles. In addition, the silica walls may play a role in preventing sintering.

CO (14.5)	He (8.2)	CO+He	Counts (75 % CO)	
75.4	24.6	94.5	6222065	
74.9	25.4	94.6	6234624	
74.8	25.4	94.5		
75.03333	**25.13333**	**94.53333**	**6228345**	0.793651
CO (7.4)	He (19.9)	CO+He	Counts (40 % CO)	
40.5	60.4	95.3	3187513	
40.5	60.5	94.9	3182006	
40.4	60.5	94.9		
40.46667	**60.46667**	**95.03333**	**3184760**	0.431579
CO (4.3)	He (24.7)	CO+He	Counts (25 % CO)	
25.6	75.9	97	1816344	
25.5	75.5	94.8	1818053	
25.3	75.3	96.5		
25.46667	**75.56667**	**96.1**	**1817199**	0.265625
CO (1.3)	He (29.4)	CO+He	Counts (10% CO)	
9.98	90.7	93.5	400122	
10.1	89.6	92.8	401286	
9.98	89.7	93.6		
10.02	**90**	**93.3**	**400704**	0.107527

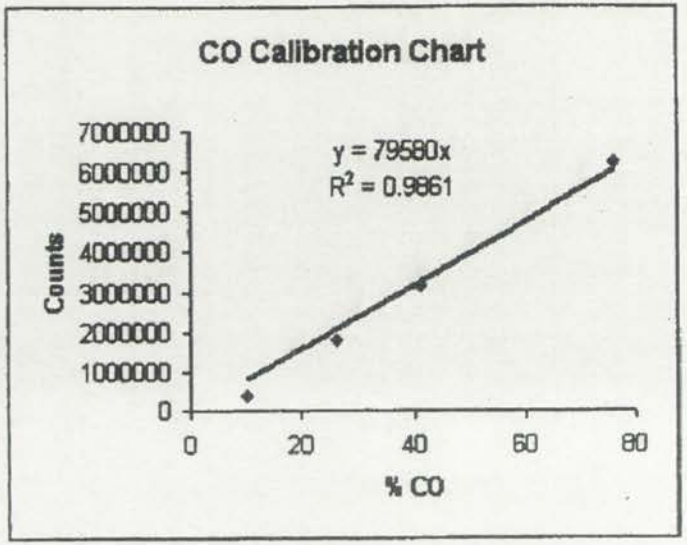

76	6228345
41	3184760
26	1817199
10	400704

5.069289	**403414**	5 % CO/He Tank

5% CO (14.5)	Counts
101	404418
104	401702
104	404123
103	403414.3

References

Arbiol J., Cabot A., Morante J.R., Fanglin C., Liu M., Applied Physics Letters, 81 (18), 3449, 2002.

Chen M, Schmidt I.D., J. of Catal., 55, 348, 1978.
Holmgren A., Azarnoush F. Fridell E., Applied Catalysis B: Environmental 22, 49, 1999.

Beck J.S., Vartuli J.C., W.J. Roth, M.E. Leonowicz, Kresge C.T., Schmitt K.D. Chu C., Olson D.H., Sheppard E.W., McCullen S.B., Higins J.B., and Schlenker J.L., J. Am. Chem. Soc., 114, 10834, 1992.

Bore M.T., Ward T.L., Fukuoka A., and Datye A.K., Catalysts Letters, 98 (4), 167, 2004.

Boudart M., Chem. Rev., 95, 661, 1995.

Cant N.W., Hicks P.C., Lennon B.S., Journal of Catalysis, 54, 372, 1978.

Ertl G., Knozinger H., Weitkamp J., Handbook of Heterogeneous Catalysis, Vol. 2, Weinheim: VCH, pp. 439-450, 1997.

Fukuoka A., Sakamato Y. Higuchi T., Kimua J., Ichikawa M., J. Phys. Chem. B, 108, 853, 2004.

Fukuoka A., Higashimoto N., Sakamoto Y., Inagaki S., Fukushima Y., Ichikawa M., Microporous and Mesoporous Materials, 48, 171, 2001a.

Fukuoka A., Higashimoto N., Sakamoto Y., Sasaki M., Sugimoto N., Fukushima Y., Ichikawa M., Catalysis Today, 66, 23, 2001b.

Guo X., Yan C., Liu P., Cheng M., Chao K., Crystal Growth and Design, 5(1), 33, 2005.

Gurdag G., Hahn T., Applied Catalysis A: General 192, 51, 2000.

Han Y., Kim J. M., Stucky J. D., Chem. Mater., 12, 2068, 2000.

Kim D.H., Lim M.S., Applied Catalysis A: General 224, 27, 2002.

Liu Z., Sakamoto Y., Ohsuna T., Hiraga K., Terasaki O., Ko C. H., Shin H. J., Ryoo R., Angew. Chem.Int. Ed., 39(17), 3107, 2000.

Mergler Y.J., Aalst A., Delft J., Nieuwenhys B.E., Applied Catalysis B: Environmental, 10, 245, 1996.

Rioux R.M., Song H., Hoefelmeyer J.D., Yang P., and Somerjai G.A., J. Phys. Chem. B 109, 2192, 2005.

Sakai M., Osada M., Sugimoto N., Inagaki S., Fukushima y., Fukuoka A., Ichikawa M., Microporus and Mesoporous Materials, 21, 597, 1998.

Shin H.J., Ryoo R., Liu Z., Terasaki O., J. Am. Chem. Soc., 123, 1246, 2003.

Terasaki O., Liu Z., Ohsua T., Shin H.J., Ryoo R., Microscopy and Microanalysis, 8, 35, 2002.

Vannice M. A., Benson J. E., Boudart M., Journal of Catasis, 16, 348, 1969.

Webb P.A., Orr C., Analytical Methods in Fine Particle Technology. Micromeritics Instrument Corp. USA. 1997.

Xia Y., Yang P., Yugang S., Wu Y., Mayers B., Gates B., Yin Y., Kim F., Yan H., Advanced Materials Review, 15(5), 353, 2003

Zhao D., Huo Q., Feng J., Chmelka B.F., and Stucky G.D., J. Am. Chem. Soc. 120, 6024, 1998.

Zou W., Gonzalez R.D., Applied Catalysis A: General, 102, 181, 1993.